Preparation of ZIF-67 Derived Quaternary Composites as Electrode Materials for Supercapacitor

By

Rabbia Naz

Reg. No. 00000330655

Session 2020-22

Supervised by

Dr. Ghulam Ali

US-Pakistan Center for Advanced Studies in Energy (USPCAS-E)

National University of Sciences and Technology (NUST)

H-12, Islamabad 44000, Pakistan

April 2023

Preparation of ZIF-67 Derived Quaternary Composites as Electrode Materials for Supercapacitor

By

Rabbia Naz

Reg. No. 00000330655

Session 2020-22

Supervised by

Dr. Ghulam Ali

A Thesis Submitted to the US-Pakistan Center for Advanced Studies in Energy in partial fulfillment of the requirements for the degree of MASTER of SCIENCE in Energy Systems Engineering

US-Pakistan Center for Advanced Studies in Energy (USPCAS-E)

National University of Sciences and Technology (NUST)

H-12, Islamabad 44000, Pakistan

April 2023

THESIS ACCEPTANCE CERTIFICATE

Certified that final copy of MS/MPhil thesis written by **Ms. Rabbia Naz** (Registration No. 00000330655), of US-Pakistan Center for Advanced Studies in Energy (USPCAS-E) has been vetted by undersigned, found complete in all respects as per NUST Statues/Regulations, is within the similarity indices limit and is accepted as partial fulfillment for the award of MS degree. It is further certified that necessary amendments as pointed out by GEC members of the scholar have also been incorporated in the said thesis.

Signature: _____

Name of Supervisor: _____

Date: _____

Signature (HOD): _____

Date: _____

Signature (Dean/Principal): _____

Date: _____

Certificate

This is to certify that work in this thesis has been carried out by **Ms. Rabbia Naz** and completed under my supervision in Synthesis, Energy Storage laboratory, and Advance Energy Materials Laboratory, US-Pakistan Center for Advanced Studies in Energy (USPCAS-E), National University of Sciences and Technology, H-12, Islamabad, Pakistan.

Supervisor: _____
Dr. Ghulam Ali
USPCAS-E
NUST, Islamabad

GEC member 1: _____
Prof. Dr. Naseem Iqbal
USPCAS-E
NUST, Islamabad

GEC member 2: _____
Dr. Sehar Shakir
USPCAS-E
NUST, Islamabad

GEC member 3: _____
Dr. Mustafa Anwar
USPCAS-E
NUST, Islamabad

HOD-ESE: _____
Dr. Rabia Liaquat
USPCAS-E
NUST, Islamabad

Dean/Principal: _____
Prof. Dr. Adeel Waqas
USPCAS-E
NUST, Islamabad

Dedication

To my parents, who supported me in every aspect of life, my siblings and friends.

Acknowledgments

First and foremost, I am thankful to **Almighty ALLAH** who is the creator and author of knowledge. Indeed, without YOUR blessings, this task would not have been possible. And I acknowledge that without YOUR willingness and guidance, I would not have done a single task. I am grateful to my parents for their unconditional love and sacrifices. your debt for your encouragement, financial and moral support. Thank you for keeping confidence in me.

Dr. Ghulam Ali, I express my sincerest gratitude to you for this opportunity, for your teaching, mentorship, and patience throughout the research. It has been truly a privilege to work with you. I would like to thank my GEC members **Prof. Dr. Naseem Iqbal, Dr. Mustafa Anwar,** and **Dr. Sehar Shakir** for their guidance and help throughout my research.

I am also thankful to the staff of Synthesis and Energy Storage Lab specially **Engineer Naveed Ahmed,** and Advanced energy materials lab engineer **Mr. Nisar Ahmad and Mr. Amir Satti** who helped in my research and gave valuable advice during my experimentation. I am also grateful to the other lab staff, faculty members, and administration who were a part of this journey. Also, all my friends, including **Iqra Shaukat, Maryam Raza, Muhammad Arslan Raza, Haseeb Ahmed, and Syeda Afsheen Zahra** for their support both academically and in general. And to life, an extraordinary experience with so many things to enjoy within a short span. Thank you for giving me so much in the years past, and for more to discover in the years to come.

Abstract

A quaternary composite has been synthesized from metal-organic frameworks (MOFs), one of the widely used precursors for the development of electrode material for supercapacitors. ZIF-67 template has been synthesized using a typical co-precipitation method followed by addition of titania in a solvothermal reactor. Three quaternary composites derived from ZIF-67 pyrolyzed at 700 ℃, 800 ℃ and 900 ℃ are synthesized using simple co-precipitation method followed by solvothermal reaction. The morphological analysis revealed a nearly globular morphology for composite prepared at temperature 900 ℃ (TZ-900). An increased degree of graphitization for carbon in thesample pyrolyzed at high temperature as confirmed using Raman spectroscopy can be attributed to better electrochemical performance. Three aqueous electrolytic media are used to study the electrochemical behavior of the prepared sample comprising 1M KOH, 1M H_2SO_4, and 1M Na_2SO_4. The prepared electrodes, TZ-700, TZ-800, and TZ-900 exhibited a specific capacitance of 303, 615, and 1617 F g^{-1} in the acidic media at 0.5 A g^{-1}. Cyclic stability run for 10,000 cycles with TZ-900 electrode showed a specific capacitance retention of 84% at a current density of 10 A g^{-1}. X-ray photoelectron spectroscopy and transmission electron microscopy further helped to examine the synergistic effect of metallic cobalt, Co (II), Co (III) and titanium ions in the nano-graphitic carbon matrix.

Keywords: *Nanographitic carbon; titania; quaternary composite; co-precipitation; hydrothermal; high specific capacitance; synergic effect.*

Table of Contents

List of Figures

List of Tables

List of Publication

ZIF-67 and Titania Derived Quaternary Composite as Electrode for High Performance Supercapacitor

Journal: Electrochimica Acta

Status:Under Review

List of Abbreviations

SCs	Supercapacitors
EDLC	Electric double layer capacitance
C	Carbon
2mim	2-methyle imidazole
GO	Graphene oxide
rGO	Reduced graphene oxide
ZIF	Zeolitic imidazolate framework
MOF	Metal organic framework
NGC	Nanographitic carbon
MOs	Metal oxides
CNT	Carbon nanotubes
Li-ion	Lithium ion
DMF	Dimethyl formamide
XRD	X ray Diffraction
XPS	X ray Photoelectron Spectroscopy
TGA	Thermogravimetric analysis
SEM	Scanning Electron Microscopy
TEM	Transmission Electron Microscopy
EIS	Electrochemical impedance spectroscopy
CV	Cyclic voltammetry
CP	Chronopotentiometry
GCD	Galvanic Charge Discharge
C	Capacitance
m	Mass loading
FTIR	Fourier transform infrared spectroscopy
EDS	Energy dispersive X-ray spectroscopy
V	Voltage

Chapter 1: Introduction

1.1 Supercapacitors

Supercapacitors are a type of energy storage device, capable of storing and releasing energy rapidly, making them a promising alternative to traditional batteries. These devices have gained significant attention in past years due to their high-power density, fast charging capability, long cycle life, and low self-discharge rates. Supercapacitors are electrochemical devices that store energy by means of an electrostatic field. The electrodes are usually made of activated carbon or other high-surface-area materials, which provide a large surface area for the electrostatic charge to accumulate. The separator is a thin layer of material that prevents the electrodes from coming into contact, while allowing ions to pass through. The electrolyte is the medium that conducts ions between the electrodes. One of the key advantages of supercapacitors over traditional batteries is their ability to charge and discharge rapidly. While batteries typically take hours to charge, supercapacitors can be charged in a matter of seconds or minutes. Meaning they can be charged and discharged many more times before degrading. This makes them a more sustainable and cost-effective solution in certain applications, such as energy storage for electric vehicles.

Supercapacitors offer several advantages over traditional batteries, including high power density, long cycle life, fast charging, and low self-discharge rates. As research and development in this field continues to advance, supercapacitors have the potential to revolutionize energy storage and contribute to a more sustainable future [1].

1.2 Background

Supercapacitors, also known as ultracapacitors, have emerged as a promising energy storage technology in recent years. The concept of supercapacitors can be traced back to the early 1950s, when researchers first discovered the phenomenon of double-layer capacitance, in which charge accumulates at the interface between a higher surface area electrode and an electrolyte.

The first commercial application of supercapacitors was in the form of static random-access memory (SRAM) backup power supplies in the 1980s. Since then, supercapacitors have been used in a number of applications, including regenerative braking systems in hybrid electric vehicles, grid-scale energy storage, and peak power shaving in renewable energy systems.

One of the main advantages of supercapacitors is their ability to store and deliver energy rapidly. They are capable of charging and discharging in a matter of seconds, which makes them particularly useful for applications that require high power densities and quick response times. Despite these advantages, the energy density of supercapacitors is still lower than that of traditional batteries, which limits their application in certain areas. However, ongoing research and development is focused on improving the supercapacitors energy density, as well as reducing their cost, in order to make them more competitive with traditional energy storage technologies [2].

Overall, supercapacitors represent a promising technology for energy storage, with potential applications in a wide range of fields. As research continues to advance, supercapacitors are likely to play a role in providing the demands of world's growing energy needs in a sustainable as well as in cost-effective manner [3].

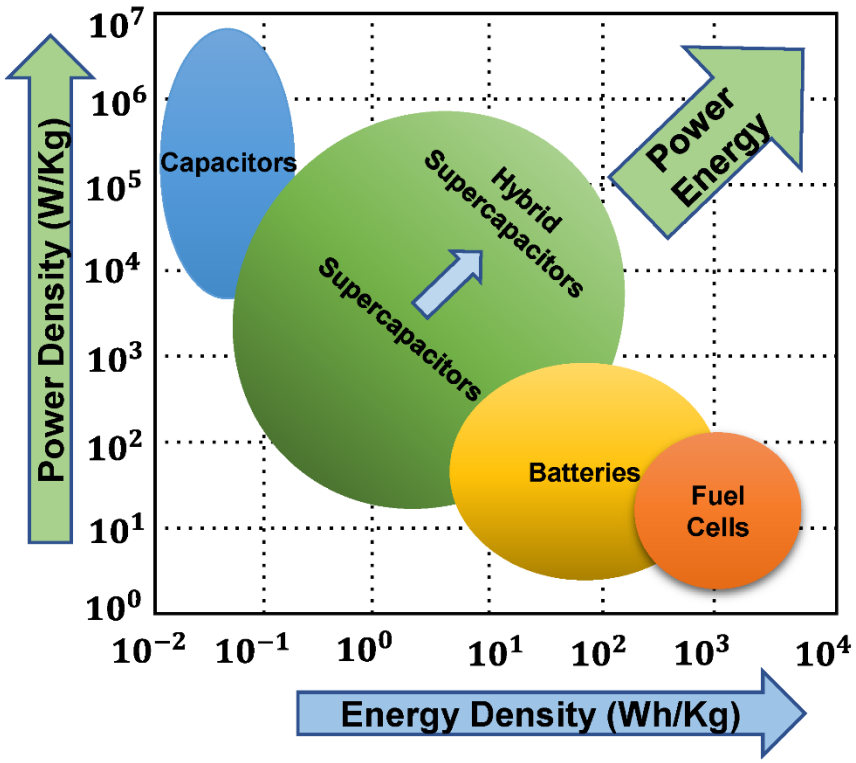

Figure 1-1. Ragone plot for Specific energy vs Specific power [4].

Depending on how they store energy, supercapacitors fall into two categories.

1.2.1 Electrical double layer capacitor (EDLC)

EDLC, or Electric Double-Layer Capacitor, is a type of supercapacitor that is designed to store electrical energy through the separation of charge at the interface between an electrode and an electrolyte. Unlike capacitors that store energy in an electric field between two conductive plates, EDLC supercapacitors use high surface area electrodes coated with a porous material to create a large interface area between the electrode and electrolyte. EDLC supercapacitors also have some limitations, such as lower energy density compared to batteries and a tendency to self-discharge over time. Researchers are currently working to improve the energy density and reduce self-discharge of EDLC supercapacitors, which could lead to even wider applications in the future [5].

1.2.2 Pseudocapacitors

Pseudocapacitors are an interesting type of electrochemical supercapacitor to store energy using reversible faradaic redox reactions, in addition to the non-faradaic charge storage

mechanisms that are utilized by conventional capacitors. These redox reactions involve reversible electron transfer between the electrode and the electrolyte, resulting in the formation of an electrical double layer and/or the formation of a solid-state pseudocapacitive material on the electrode surface.

Pseudocapacitors have a number of advantages over traditional capacitors and EDLC supercapacitors, including higher energy density and better long-term stability. They are commonly made from materials such as transition metal oxides and/or conducting polymers, which have high specific capacitance due to their pseudocapacitive behavior. They are especially useful in situations where both high power and high energy density are required [5].

1.3 Working of a supercapacitors

There are two different kinds of them when it comes to energy storage. EDLC is one type, and pseudocapacitors is another. Both types operate using various chemistry. The electrode surface stores electrostatic charge in EDLC.

1.3.1 Working Mechanism Pseudocapacitor

In The electrodes of pseudocapacitors are made from materials with high pseudocapacitance, which is the ability of a material to store and release electrical charge through redox reactions. These materials include transition metal oxides, polymers, and other materials with high specific capacitance. The electrolyte used in pseudocapacitors is typically an aqueous or organic solution containing ions that can participate in the redox reactions at the electrode surface. When a voltage is applied to the pseudocapacitor, charge separation occurs at the electrode and electrolyte interface. The reactions that take place result in the formation of a solid-state pseudocapacitive material on the surface of the electrode, which stores electrical charge. The charge stored in the pseudocapacitive material can be discharged rapidly, providing high power output [6].

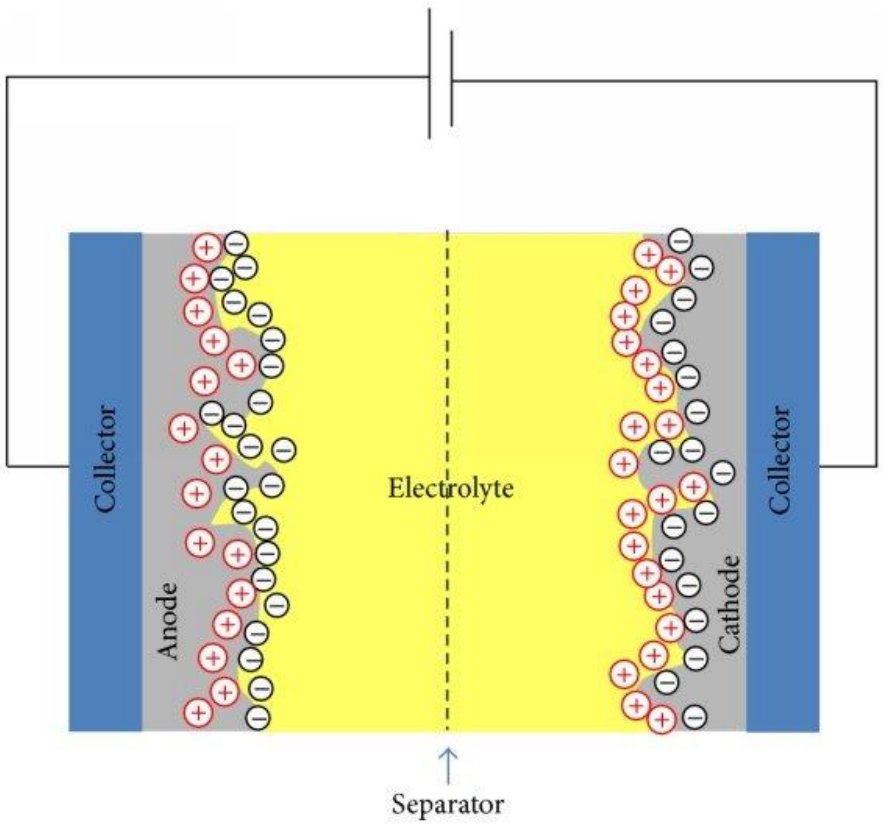

Figure 1-2. Construction of a simple capacitor [7].

In a traditional capacitor, the electric charge is retained in the intensive electric field among two conducting sheets, which are isolated by an insulator. Figure 1.2. As a result of their small plate area and geometrically constrained separation distance, conventional electrostatic capacitors store relatively little energy. Supercapacitors based on the EDL mechanism can store significantly more energy due to the vast interfacial area and atomic charge split gaps. Helmholtz and Chapman's earlier studies on EDL mode were the basis for Stern's EDL mode development and modification in the 1920s.

Stern mode recognized two distinct ion distribution regions: the inner compact layer, and the outer diffuse layer as shown in Figure 1.3. The electrode strongly adsorbs hydrous ions in compact layer. Specific ions in the interior Helmholtz plane (IHP) and nonspecific counterions in the exterior Helmholtz plane (OHP) comprise the compact layer. As a result of thermal motion in the electrolyte solution, an electrolyte diffuse layer forms around an electrode [8].

In equation (1) C_{dl} is EDL capacitance, C_H is compact capacitance and C_{diff} is diffusion capacitance.

$$\frac{1}{C_{dl}} = \frac{1}{C_H} + \frac{1}{C_{diff}} \quad (1)$$

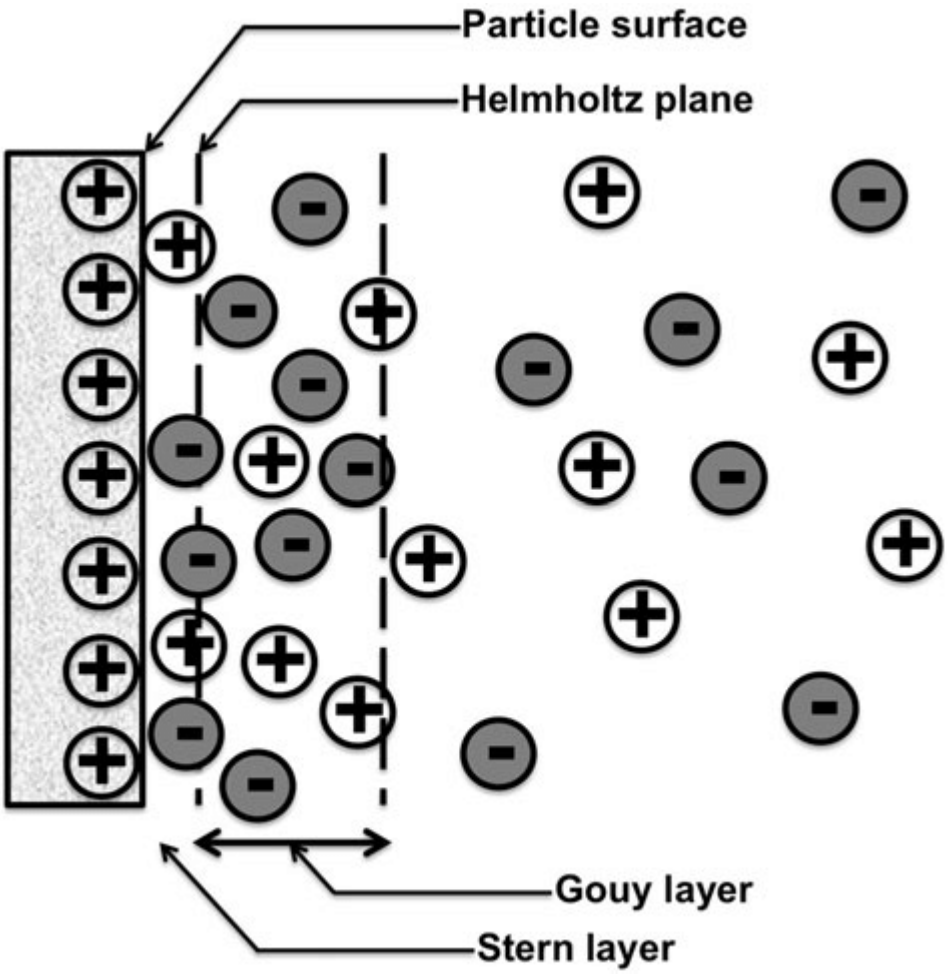

Figure 1-3. Helmholtz Plane and Gouy Layer in Stern model [9].

A thermodynamically induced pseudo capacitance differs from the EDL capacitance. On the electrode materials of a pseudo capacitor, redox faradic reaction transpires, and charge is passed across the electrode/electrolyte interface. A pseudo-faradaic capacitor's processes, on the other hand, are liable to a thermodynamic discrepancy in potential

throughout charge buildup, making them more reversible as well as more powerful. Faradaic processes occur at pseudocapacitive electrodes in three different ways:

- Adsorption of H^+ from the electrolyte that is reversible in nature.
- Ions from the electrolyte are involved in redox reactions.
- Conducting polymer-based electrodes with reversible doping and deducing processes [10].

1.3.2 Working Mechanism of EDLC

In the two-plate EDLC capacitor, the electrode-to-electrolyte contact (Figure 1. 4) depicts the location of the charging accumulator. While charging, electrons are transferred from the negative to the positive electrodes through the outer loop. For unknown reasons, cations and anions in electrolytes are attracted to the negative & positive electrodes. During discharge, there are two opposing forces at work during discharge: electrons and ions. No charge is transferred in the supercapacitor of the EDLC, and the pseudocapacitors are shown in Figure 1. 4. The redox reaction takes place on the electrode, resulting in the creation of charges and the transfer of these charges between the two layers. Due to the lower power density of Faradaic systems, EDLC's power density may be lower than that of pseudocapacitors. Because pseudocapacitors are a Faradaic device, they often have a larger specific capacity and energy density than EDLC.

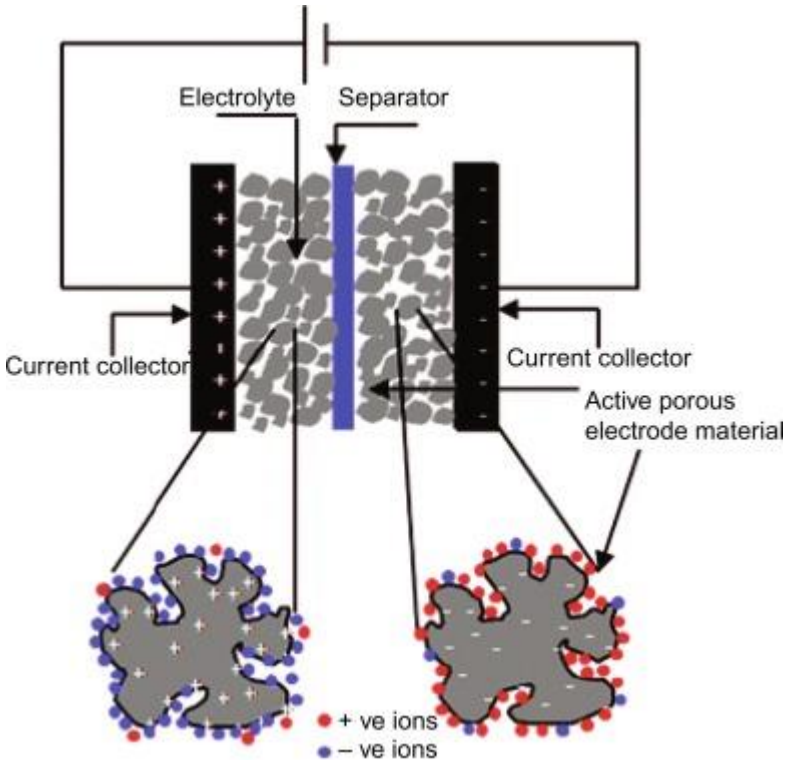

Figure 1-4. Representation of EDLC (high surface area porous electrode is used) [11].

Figure 1. 5 illustrates how voltage is applied to the capacitor causing opposing charges to be collected on each electrode, which creates an eclectic field that lets the capacitor store energy. The capacitance of a system, C, may be written as:

$$C = \frac{Q}{V}$$

Q stands for the stored charges, while V stands for the applied voltage. The capacitance C is governed by the electrode surface area and inversely proportional to the electrode's distance. Hence, capacitance can be as:

$$C = \varepsilon_o \varepsilon_r \frac{Q}{V}$$

ε_r is the isolating substance between the electrodes, and ε_o is the dielectric constant, always with relative permittivity. Using Eqs. (1) and (2), a supercapacitor's output is determined by its energy and power density. Power density increases with supercapacitor charge processing. At electrode/electrolyte contacts, EDLs generate electrostatic interactions. Charge on the electrode surface determines capacitance.

Redox reactions are typically attended by an EDL capacitance part that is relative to the electrochemically comprehensible interface area.

Carbon surfaces with functional groups, organic polymers (Polypyrrole PPy), and transition metal oxides for instance (nickel, iron, manganese) are among the most commonly known active species. When numerous oxidation states from the electrode materials can be attained pseudo capacitors can achieve very elevated energy density. Pseudocapacitors capacitance can be 10 to 100 times superior to EDLC. But sluggish faradic reactions and morphological adjustments during the operation precedes to lower specific power and life expectancy is also diminished [12].

1.4 Supercapacitors Performance Optimization

Electrode pore size is of the utmost importance when maximizing specific capacitance. Three types of pore sizes can be distinguished within the electrode material, i.e., micropores, mesopores, and macropores. Other important factors in the performance of supercapacitors involve the accessibility of these pores to the electrolyte. Micropores are keys to the adsorption and retention of ions within the double layer and 10 thus are the primary source of charge accumulation. Macropores and mesopores must be present to facilitate rapid ion movement throughout the bulk of the material. The choice of electrode material is crucial to the performance of supercapacitors. Researchers are continually exploring new materials, including graphene, metal oxides, conducting polymers, that offer high specific capacitance, low resistance, and long cycle life. If an electrode lacks an adequate number of these larger pores, it experiences larger resistance to ion flow during charging and discharging. Also, it affects the capacitance. The most highly conductive electrolyte salt with maximum mobility within its solvent will provide the highest capacitance The choice of electrolyte can also affect the performance of supercapacitors. Research is carried out to implement the use of new types of electrolytes, including ionic liquids and organic solvents, that offer high conductivity and high voltage stability. The operating conditions of supercapacitors can also affect their performance. For example, operating at lower temperatures can improve the energy density of some types of supercapacitors, while optimizing the voltage range and the charging and discharging rate can improve power density. Combining supercapacitors with other

energy storage technologies, such as batteries or fuel cells, can improve overall energy storage performance [13].

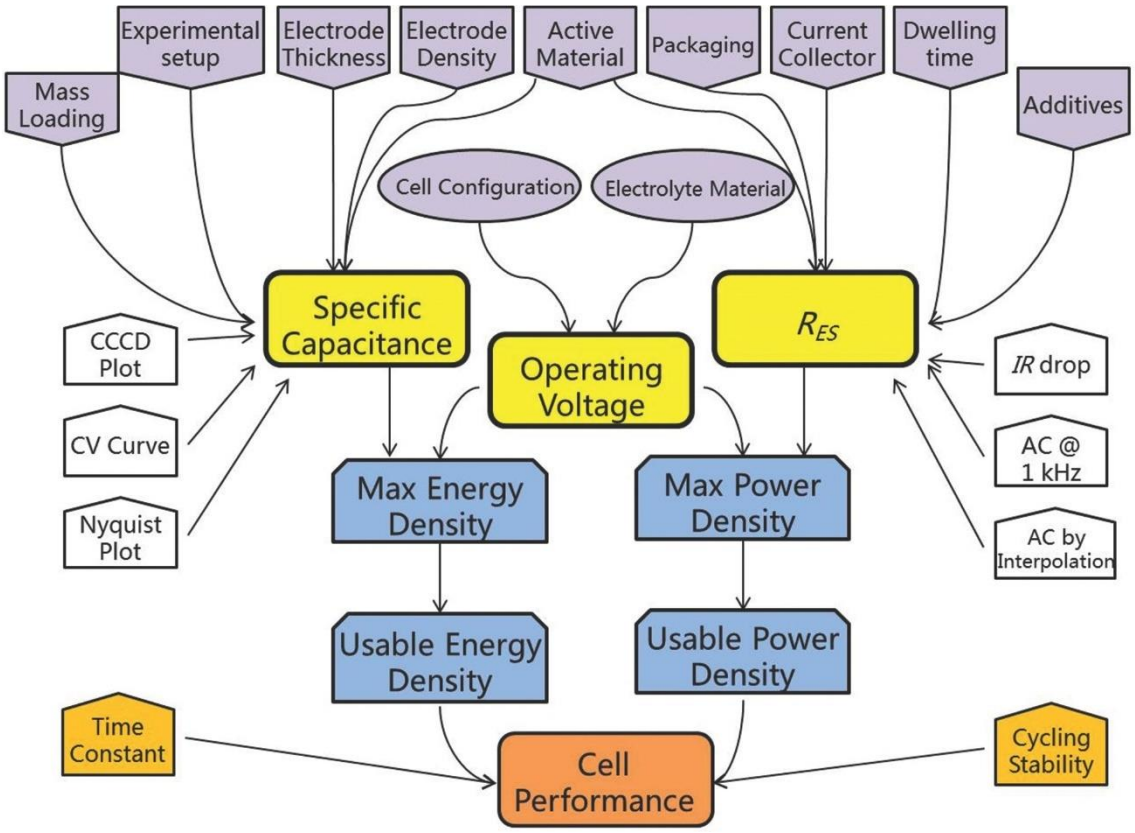

Figure 1-5. Performance Optimization of Supercapacitors [14].

1.5 Electrochemical Testing

1.5.1 Three-Electrode System

The three-electrode system is one of the common methods used for testing the performance of supercapacitors. This system consists of three electrodes namely a working electrode, a reference electrode, & a counter electrode. A working electrode is being tested and is typically made of a high surface area material, such as activated carbon. The reference electrode is used to monitor the potential of the working electrode and is typically made of a noble metal, such as platinum. The counter electrode is used to balance the charges on the working electrode and is typically made of a conductive material, such as a metal foil. The three-electrode system is commonly used for testing supercapacitor electrodes because it allows for precise measurement of electrochemical behavior and

capacitance. By using a reference electrode, it is possible to accurately control the potential of the working electrode, which is important for obtaining reliable measurements. Additionally, the counter electrode ensures that the charges are balanced, which is crucial for accurate measurement of capacitance. Importantly in three-electrode cell, the applied potential on working electrode is given according to reference electrode used and is applied totally on working electrode [15].

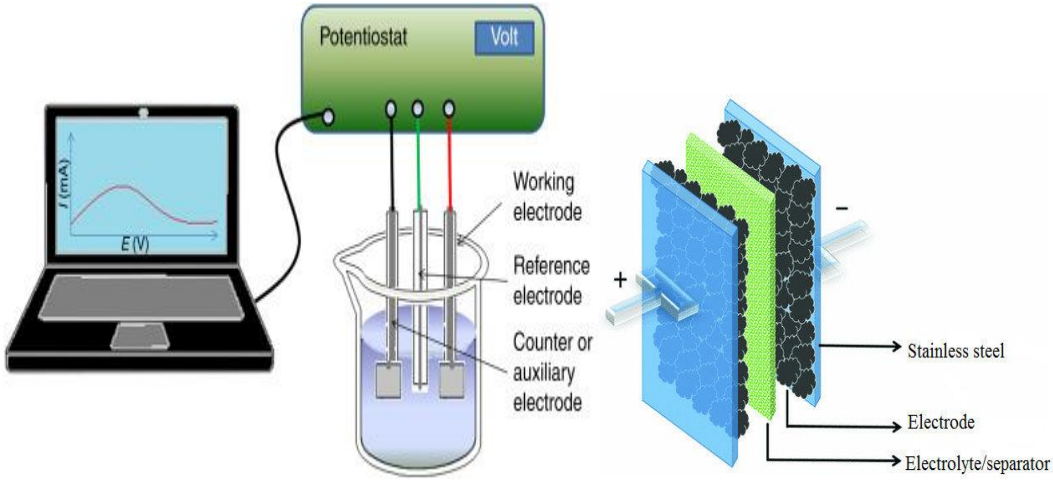

Figure 1-6. A three-electrode Beaker cell (left) and Two-Electrode System (Right) [16].

1.5.2 Two-Electrode System

As a packaged supercapacitor cell's performance is closely matched by a two-electrode test fixture, the electrochemical activity can be more accurately assessed. They can be purchased commercially or made from two stainless steel plates. A three-electrode cell allows just working electrode to be analyzed, whereas a two-electrode configuration allows to analyze both electrodes separately. Electric potential applied to the system are distributed equally to every electrode in a two-electrode cell. Accordingly, the working electrode in 3-electrode cell is subjected to two times the potential range as that of a 2-electrode cell, which results in a doubled capacitance calculation. In two electrode cell, when the RE and WE are in close proximity, the RE has the ability to accurately control the interfacial potential. These parameters are used at the packaged cell level to evaluate supercapacitor performance [17].

1.6 Problem Statement

- Pure MOFs have some drawbacks such as low conductivity and particulate aggregation, which limit their use as electrode materials.
- This results in low energy density of supercapacitors, typically less than 50 Wh/kg, compared to batteries with energy densities of 30-300 Wh/kg.
- Cyclic stability is a major concern with MOFs as electrode materials.

1.7 Objectives

- To synthesize a composite electrode material comprising Co_3O_4/Co/TiO_2/NGC for high performance supercapacitors.
- To study and analyze the electrochemical performance of electrode material in three different electrolytes.
- To analyze the cyclic stability of the best-performing electrode material.

Summary

This chapter discuss the background and comparison of all energy storage systems and compare them to supercapacitors. Further chapter 1 discusses the types and working of supercapacitors and their performance evaluation in detail.

List of References

1 Sinha, P. and K.K. Kar, *Introduction to supercapacitors*, in *Handbook of Nanocomposite Supercapacitor Materials II: Performance*. 2020, Springer. p. 1-28.

2. Samantara, A.K. and S. Ratha, *Materials development for Active/Passive components of a supercapacitor: background, present status and future perspective.* 2017.

3. Samantara, A.K., et al., *Historical background and present status of the supercapacitors.* Materials development for active/passive components of a supercapacitor: background, present status and future perspective, 2018: p. 9-10.

4. Wayu, M., *Manganese oxide carbon-based nanocomposite in energy storage applications.* Solids, 2021. **2**(2): p. 232-248.

5. Lakal, N., S. Dubal, and P. Lokhande, *Supercapacitors: An introduction.* Nanotechnology in the Automotive Industry, 2022: p. 459-466.

6. Bhojane, P., *Recent advances and fundamentals of Pseudocapacitors: Materials, mechanism, and its understanding.* Journal of Energy Storage, 2022. **45**: p. 103654.

7. Saleem, A.M., V. Desmaris, and P. Enoksson, *Performance enhancement of carbon nanomaterials for supercapacitors.* Journal of Nanomaterials, 2016. **2016**.

8. Jadhav, V.V., et al., *Electrochemical supercapacitors: history, types, designing processes, operation mechanisms, and advantages and disadvantages.* Bismuth-Ferrite-Based Electrochemical Supercapacitors, 2020: p. 11-36.

9. Piacenza, E., A. Presentato, and R.J. Turner, *Stability of biogenic metal (loid) nanomaterials related to the colloidal stabilization theory of chemical nanostructures.* Critical reviews in biotechnology, 2018. **38**(8): p. 1137-1156.

10. Khot, M. and A. Kiani, *A review on the advances in electrochemical capacitive charge storage in transition metal oxide electrodes for pseudocapacitors.* International Journal of Energy Research, 2022.

11. Yin, L., et al., *Ionic liquid electrolytes in electric double layer capacitors.* Sci. China Mater, 2019. **62**(11): p. 1537-1555.

12. Najib, S. and E. Erdem, *Current progress achieved in novel materials for supercapacitor electrodes: mini review.* Nanoscale Advances, 2019. **1**(8): p. 2817-2827.
13. Wu, S., et al., *A review of performance optimization of MOF-derived metal oxide as electrode materials for supercapacitors.* International Journal of Energy Research, 2019. **43**(2): p. 697-716.
14. Zhang, S. and N. Pan, *Supercapacitors performance evaluation.* Advanced Energy Materials, 2015. **5**(6): p. 1401401.
15. Gou, Q., et al., *Recent advances on boosting the cell voltage of aqueous supercapacitors.* Nano-Micro Letters, 2020. **12**: p. 1-22.
16. Jänes, A., H. Kurig, and E. Lust, *Characterisation of activated nanoporous carbon for supercapacitor electrode materials.* Carbon, 2007. **45**(6): p. 1226-1233.
17. Zhu, C., et al., *All metal nitrides solid-state asymmetric supercapacitors.* Advanced Materials, 2015. **27**(31): p. 4566-4571.

Chapter 2: Literature Review

2.1 Electrode Materials

The choice of electrode materials significantly affects the charge storage with final capacitance of a supercapacitor. For optimal capacitance, the crucial factor is the effective surface area and electrical conductivity of the electrode material. Carbon-based materials, such as graphite, graphene, carbon nanotubes, & activated carbon, are preferred as electrode materials due to their ability to store charge via electrical double-layer capacitance on their surface. To achieve high capacitance, the material should have high surface area, appropriate pore size and distribution, and functional groups. Other materials that are also suitable for supercapacitor electrode materials include metal oxides, polymers, metal-organic frameworks, phosphorus, MXenes, and metal nitrides [1]. To ensure optimal performance, the electrode materials should possess several key properties. Firstly, they should have a high surface area to have more sites resulting in better charge storage. Additionally, good electrical conductivity is critical to ensure efficient charge transfer between the electrode and the electrolyte. Pore size of the electrode material also affects its performance, with appropriate pore size allowing for better ion diffusion and charge transfer. A uniform pore size distribution is also essential to ensure that the electrolyte penetrates the electrode material uniformly, leading to better performance. The presence of functional groups such as oxygen-containing groups enhances the electrochemical performance of the electrode material. Furthermore, the electrode material should be chemically stable in the electrolyte to prevent degradation and loss of performance over time. Finally, the cost and abundance of the electrode material are important considerations as they affect the overall cost of the supercapacitor device and its mass production [2].

2.2 Categories of Electrode Materials

Electrode materials for supercapacitors can be broadly classified into two categories: carbon-based materials and pseudocapacitive materials.

Carbon-based materials include activated carbon, graphene, graphite, and carbon nanotubes, are the most commonly used electrode materials for supercapacitors due to their high surface area and good electrical conductivity. They store charge through the electrical double-layer capacitance (EDLC) mechanism, which involves the accumulation of ions at the electrode-electrolyte interface.

Pseudocapacitive materials store charge through surface redox reactions, which involve the reversible transfer of electrons between the electrode and the electrolyte. These materials typically have a lower surface area than carbon-based materials but can achieve higher capacitance due to their ability to store charge through both EDLC and pseudocapacitance mechanisms. Examples of pseudocapacitive materials include metal oxides, conducting polymers, and transition metal dichalcogenides.

Another category of electrode materials for supercapacitors is hybrid materials, which combine the properties of both carbon-based and pseudocapacitive materials. These materials can offer the benefits of high capacitance and high power density. Some examples of hybrid materials include carbon nanotube-metal oxide composites, graphene-metal oxide composites, and conducting polymer-metal oxide composites.

The choice of electrode material depends on the specific application and desired performance characteristics of the supercapacitor device.

MOFs have a tunable surface area, pore size, and a huge range of functional groups, which make them attractive for various applications such as gas storage, catalysis, and sensing. In recent years, MOFs have also gained significant attention as potential electrode materials for energy storage devices such as supercapacitors and batteries. MOFs can store charge through various mechanisms such as pseudocapacitance, double-layer capacitance, and redox reactions, depending on the metal ion and ligand used. They have shown promising electrochemical performance with high capacitance & good cycling stability, and fast charge-discharge rates. However, there are still some challenges that need to be addressed for practical applications of MOFs in energy storage devices. One major challenge is their poor conductivity, which can limit their charge transfer kinetics and overall electrochemical performance. Various strategies such as doping, hybridization with conductive materials, and structural modification have been proposed to improve the conductivity of MOFs. Overall, MOFs are a promising class of materials for energy

storage applications, and their unique properties and versatility continue to attract attention from the scientific community [3].

2.3 Carbon based composites

Carbon-based materials are a class of materials that are composed primarily of carbon atoms. They have a wide range of properties and applications, including their use as electrode materials for supercapacitors. Carbon-based materials are attractive electrode materials for supercapacitors due to their abundance, low cost, and excellent electrochemical properties. They can store charge through the electrical double-layer capacitance (EDLC) mechanism, which involves the accumulation of ions at the electrode-electrolyte interface, and can also exhibit pseudocapacitive behavior through surface redox reactions. Various modifications and combinations of carbon-based materials have been proposed to enhance their electrochemical performance and tailor their properties for specific applications [4].

2.3.1 Activated Carbon (AC)

It is made by heating carbon-rich materials like coconut shells, wood, or coal at high temperatures while a gas or activating agent is present. This causes the carbon to develop a network of pores on its surface. These pores offer a sizable surface area for effective ion transport and charge storage. By adjusting the raw material and activation parameters, such as temperature, duration, and kind of activating agent, activated carbon's qualities can be tailored. As a result, activated carbons with customized characteristics for particular applications can be produced. However, activated carbon can suffer from limited capacitance and poor stability at high voltages, which can limit its performance in some applications. Various modifications and combinations of activated carbon with other materials have been proposed to overcome these limitations and enhance its electrochemical performance [5].

2.3.2 Carbon nano tubes (CNTs)

CNTs are synthesized as a result of sp2 hybridization, graphene sheets are wrapped in covalently bonded carbon atoms. In terms of single-walled CNTs (SWCNTs) and porosity, graphene sheets are classified by the number of layers and porosity. That deliver mechanical potency and conductivity to the complex material. After 50,000 cycles in

aqueous electrolyte solutions, supercapacitor electrode that has CNT dopped composite showed negligible capacitance fading. Same system without using CNTs couldn't compete with it and exhibits a decline in capacitance after 30,000 cycles. (Figure 2.1) [6]. Compared to CNTs combined with GQDs, these composites produced better results (200 mF/cm^2 vs 0.44 mF/cm^2). Graphene, despite its intriguing properties, is still a long way from being used as electrodes in practical energy storage devices, as this study shows.

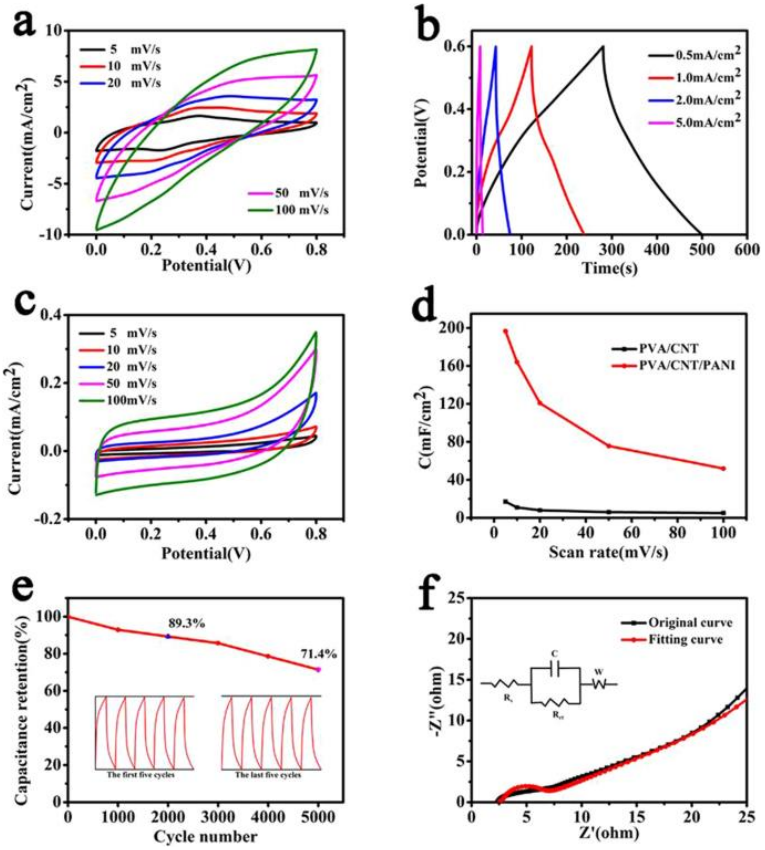

Figure 2-1. (a, b, c, f) Cyclic voltammetry, gravimetric Charge/Discharge and Nyquist plot of carbon-based polymer electrodesin 3M KOH electrolyte (d) Carbon based polymer electrode with CNTs (e) Capacity vs. cycle number plot [6]

Carbon nanotubes (CNTs) presence within the $CuCo_2S_4$ matrix created a multitude of effective pathways for electron transfer & ion diffusion, which ultimately enhanced the faradaic reactions at the $CuCo_2S_4$ electrode during energy storage. At 1 A g^{-1}, the $CuCo_2S_4$/CNTs-3.2% electrode delivered a specific capacitance of 557.5 F g^{-1}, which was significantly higher than that of the pristine $CuCo_2S_4$ electrode having 373.4 F g^{-1} and the CuO/Co_3O_4/CNTs-3.2% electrode with 356.5 F g^{-1}. To evaluate its energy storage

potential, an asymmetric supercapacitor (ASC) was constructed using the CuCo2S4/CNTs-3.2% electrode as +ve electrode & active carbon is taken as negative electrode. The ASC demonstrated an energy density of 23.2 Wh kg^{-1} at a power density of 402.7 W kg^{-1}. Furthermore, even after 10,000 cycles, retained 85.7% of its original value, suggesting exceptional cycle stability [7].

Wu et al. has presented a straightforward technique for manufacturing large-scale, self-standing film electrodes of composites for supercapacitors composed of $NiCo_2O_4$@carbon nanotube (CNT). By vacuum filtering stacked $NiCo_2O_4$-CNT and CNT alternately, we fabricated $NiCo_2O_4$-CNT/CNT film electrodes. Of all the composite electrodes synthesized, the one fired in air exhibited the best electrochemical performance, delivering a specific capacitance of 1,590 F g^{-1} at j 0.5 A g^{-1} with stability. The lightweight, flexible, and self-standing film electrodes, measuring approximately 24.3 µm thick, demonstrated a high volumetric capacitance of 873 F cm^{-3} at j of 0.5 A g^{-1}. To test the practicality of these electrodes, we constructed an solid state asymmetric supercapacitor consisting of a composite film electrode with a carbon cloth electrode being treated. This supercapacitor achieved not only a high energy density of around 27.6 Wh kg^{-1} at a rate of 0.55 kW kg^{-1} but also excellent cycling stability, sustaining approximately 95% of its capacitance after 5000 cycles [8].

2.3.3 N-doped carbons

Alterations in the physiochemical, and electrochemical characteristics of carbonaceous materials can be caused by nitrogen doping carbon. Nitric acid can also modify the electronic and crystallographic arrangement of carbons to increase chemical stability as well as it enhances electrical conduction. In addition to supercapacitors and catalysis, nitrogen-doped carbons are also used in adsorption and separation processes. Most Nitrogen doped carbon materials are synthesized using N-containing precursors. Nitrogen matter in common precursors is a limiting factor in this type of synthesis. As a result of an effort to raise the nitrogen quantity in the precursors, the mesostructured of the carbons degrades. It was recently reported that carbonization, nitrogen functionalization, and activation can all be combined into one process to synthesize N-doped materials [9].

The electrospun polyacrylonitrile (PAN) is used to embed ultrafine zeolitic imidazolate framework (ZIF-8) nanoparticles, which are then carbonized to form hierarchical porous

nanofibers carbon hollow nanoparticles. The developed material, HPCNFs-N, has remarkable specific capacitance under a range of current densities, a high energy and power density with long cycling stability of over 10,000 cycles. It can be seen in the results that it provided better results in terms of multiple dimensions including capacitance. These improved properties are a result of its distinct structural characteristics and excellent chemical make-up [10].

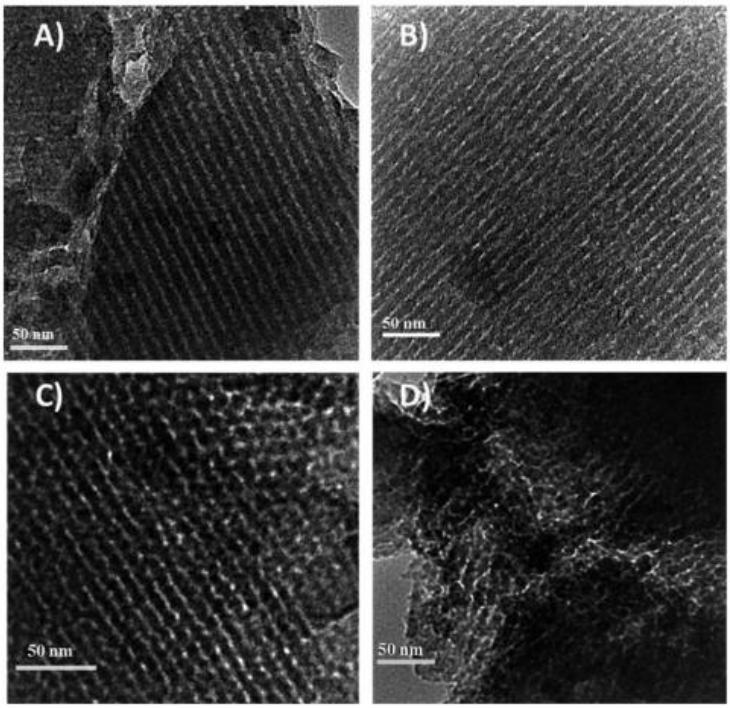

Figure 2-2. (A) TEM images of sample (A) NC0, sample (B) NC1, sample (C) NC2, and sample (D) NC3 showing Nitrogen Doped Carbon at Different Ratios [10]

A soft-templating hydrothermal method has been developed to produce nitrogen (N)-doped mesoporous carbon. The study systematically investigates the factors that impact electrochemical performance having specific surface area, ionic conductivity, and better pseudocapacitance. The optimum N-doping level for achieving high electrochemical capacitance is found to be 6.0 wt% N-doping. Three factors affecting capacitance and provides insights for the future design of electrode materials with better electrochemical performance [11].

2.3.4 Graphene composites

Two-dimensional graphene sheets are composed of carbon atoms that are connected by hexagonal networks. Graphene sheets have many advantages over other materials. In contrast, the oxidation produces' adsorption shrinks the surface area of the oxidized graphene sheets by stacking them back up again. Further activation is required to separate the graphene sheets from each other and their surface area is enhanced. As a result of high-temperature annealing, the sheets of graphene-oxide can become separated. GO/AC composites were synthesized in one step in a recent study. An eight-fold increase in surface area was observed after the composite material had been annealed. Graphene's electrochemical performance also improves, compared to graphene without active carbon. It is possible to create mesopores between microporous scaffolds by assembling graphene plates in a porous arrangement and taking advantage of graphene's large surface area. Due to this increased diffusion efficiency, the electrochemical performance is enhanced as well. Electrodes made from this composite had a three-fold higher energy density than electrodes made from pristine activated carbon [12].

The honeycomb-like lattice of carbon atoms in graphene makes it an exceptional matrix for the preparation of 2D porous materials. Porous organic materials are often assembled using Schiff-base chemistry. Supercapacitors with capacitances of 430 F g^{-1} at 0.1 A g^{-1} were made using TPP as a precursor [13].

A new arrangements of hollow carbon atoms in way that they are curved to form a curved sheet like assembly should be discussed. A curvature in the particle's morphology prevents the particles from stacking. Using silica atoms with a sturdy core and a matrix with N-rich precursor can be used to create these carbon capsules by nano casting. (Figure 2.3). These carbon capsules have a high performance in an aqueous medium, with an efficiency of 240 F/g and capacitance is retained by 72 percent after 10,000 cycles. With a current density of 100 A g^{-1} and a capacitance retention up to 93 percent after 10000 cycles, these supercapacitors perform better in an organic medium [14]. For supercapacitor electrodes, carbon-only materials have been studied for years. In addition, graphene and CNTs have a large surface area that could lead to the maximum specific EDL capacitance. These materials alone, however, present engineering challenges and produce a modest volumetric capacitance when used in practical cells.

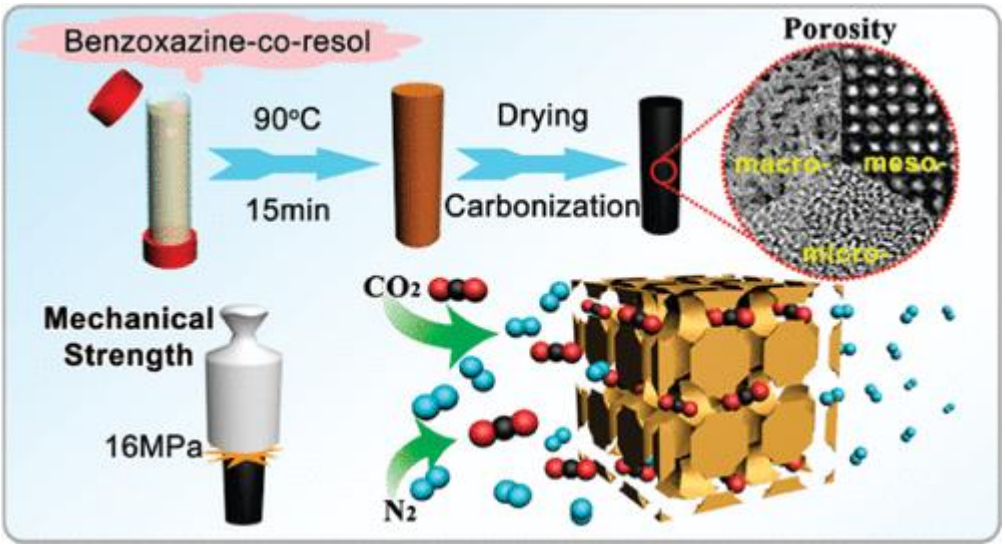

Figure 2-3. Synthesis of Carbon capsule [14].

Coupled composite structures combining different types of carbon have made great strides in the area. In addition to making practical electrodes, using such composite materials could pave the way for the fabrication of porous structures with improved properties. In some cases, carbon-based composite electrodes had capacitances that were almost double than those of carbon electrodes that were left unmodified. CNT-activated carbon composites are a great example of such an improvement and advantage. CNTs have been mixed with electrode materials for a long time. Nanofabrication methods, which allow materials to be controlled at atomic scale, and the ability to mass produce nanomaterials are promoting and advancing these approaches.

2.4 Metal-oxide composites

Supercapacitors and hybrid devices have extensively investigated a variety of metal oxides, including $Ru_2 O_3$, $V_2 O_5$, $Fe_3 O_4$, $Co_3 O_4$, $Ni_2 O_3$, and $Ti_2 O_2$. When compared to carbon materials' capacitive charge storage mechanism (EDL), metal oxides demonstrate pseudocapacitance. Activated carbon electrodes can be combined with other oxides (Co_3O_4, NiO, TiO_2) to form battery-type electrodes. In all of these oxides, the multivalent nature of their transition metals is responsible for their redox behavior. Protons and/or hydroxide anions interact well with most of these oxides because their oxidation states changes, and they occur reversible oxidation and reduction reactions that result affect both the electrode surface and the bulk of these oxides.

Most metal oxides suffer from excellent specific capacitance or capacity because they have low conductivity. All of these aspects are excellent in carbon materials, which have a relatively low specific capacitance. A composite electrode with a conductive backbone that supports nanocomponents with high capacitance/capacity may be created by integrating nano metal oxides with carbon structures [15].

2.4.1 TiO_2-based composites

A hydrothermal method is implied to synthesize TiO_2 nanotubes with reduced graphene oxide with formula TiO_2NT/RGO and a Co-doped material with TiO_2NT & RGO composites. Poly(ethylene-glycol) was used as a structure-directing agent in the solvothermal route for TiO_2NT and Co-doped TiO_2NT synthesis. The morphology and properties of the composites were studied using various techniques. A Co-doped TiO_2NT/RGO based electrode with 10.00 wt.% GO showed a specific capacitance value up to 27.5 F g^{-1} on 0.2 A g^{-1} current density in a symmetrical two-electrode cell, while TiO_2 exhibited only 0.7 F g^{-1} [16].

Due to its high surface area, porosity, mechanical strength, along with transport qualities, as well as their low cost, non-toxicity, and environmental friendliness, titanium dioxide (TiO_2) nanotube arrays have emerged as a best performing material for electrochemical energy storage systems. TiO_2 nanotubes are a favourite among researchers because of their distinctive qualities, including unidirectional electron transport and chemical and mechanical stability. Techniques for electrochemical nanofabrication have made it easier to co-deposit composite components and allowed for precise control over tube geometry. The electrochemical capacitance of titania nanotubes has been improved using a variety of techniques, including hydrogenation, nitridation, preferential crystal axis development, doping, plasma treatment, and other processes. This article examines the strategic development of TiO_2 nanotubes as a capable electrode material for supercapacitors & explores their potential in the future [17].

2.4.2 Cobalt oxide-based composites

The article describes the synthesis procedure and electrochemical properties of Co_3O_4 and rGONS composites for supercapacitors. The Co_3O_4 nanosheets, which are homogeneously assembled fine nanoparticles, are found to aggregate in a flower shape on reduced graphene oxide surfaces. Compared to pure Co_3O_4, the as-made Co_3O_4/rGONS

composites exhibit improved specific capacity and redox performance, which are related to the composite structure having high porosity formed due to Co_3O_4 with reduced graphene oxide nanosheets interaction during fabrication. The Co_3O_4/rGONS-II composite shows good cyclic performance with better coulomb efficiency and also with a specific capacitance of 400 F g^{-1} at current density (j)of 0.5-2.0 A g^{-1} [18].

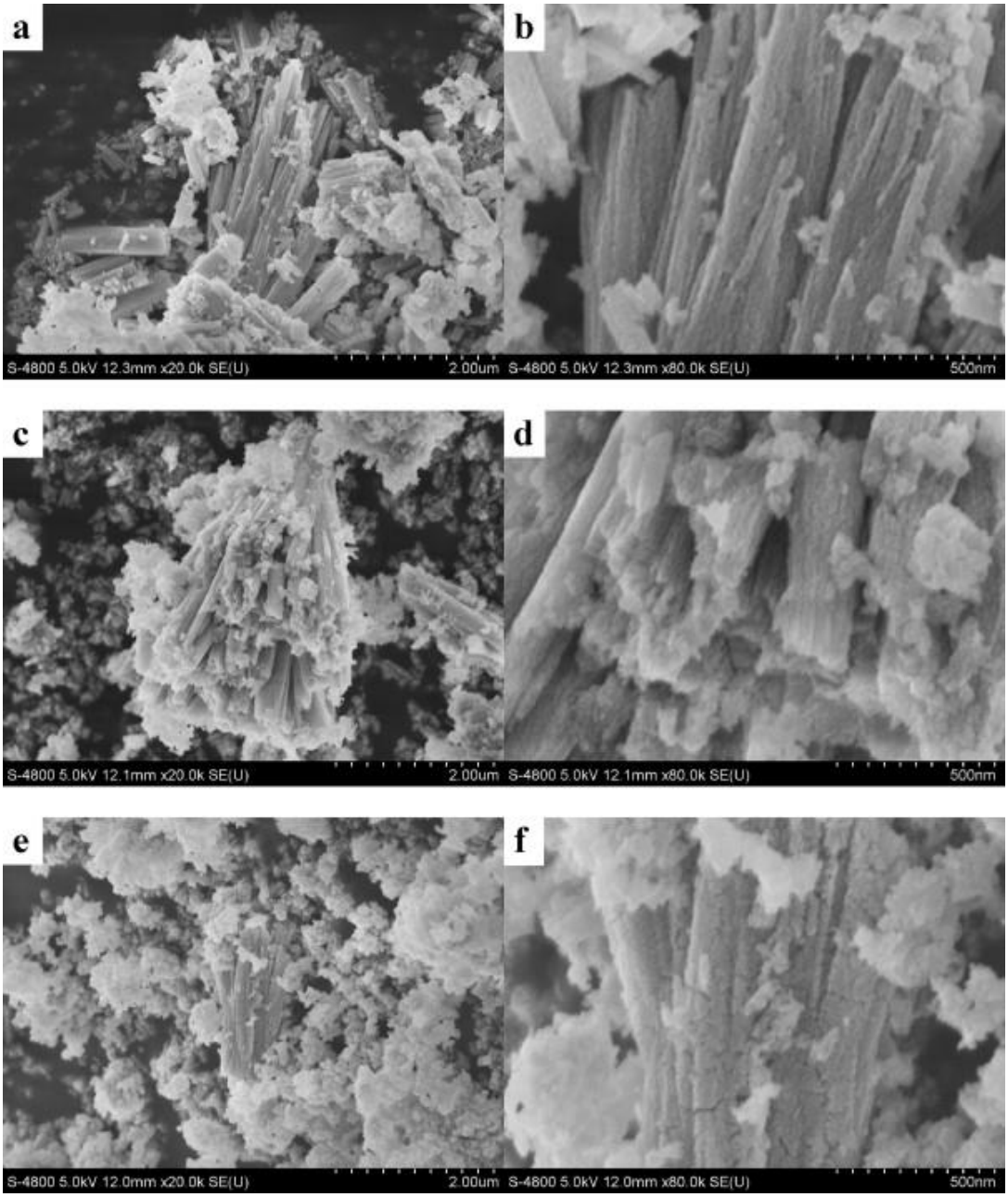

Figure 2-4. SEM images of Co_3O_4 (pure) (a, b), Co_3O_4/rGONS-II (c, d) and Co_3O_4/rGONS-IV (e, f) at different magnification [18].

This approach has acquired significant attention. As an example, the solvothermal method adopted in fabrication of an ultrafine Co_3O_4 nanoparticle material. These ultrafine Co_3O_4 nanoparticles exhibited a specific capacitance of 523.0 $F \cdot g^{-1}$ at current density 0.5 $A \cdot g^{-1}$ with a good cycling stability, and it was retained at about 104.9% after 1500 cycles [19].

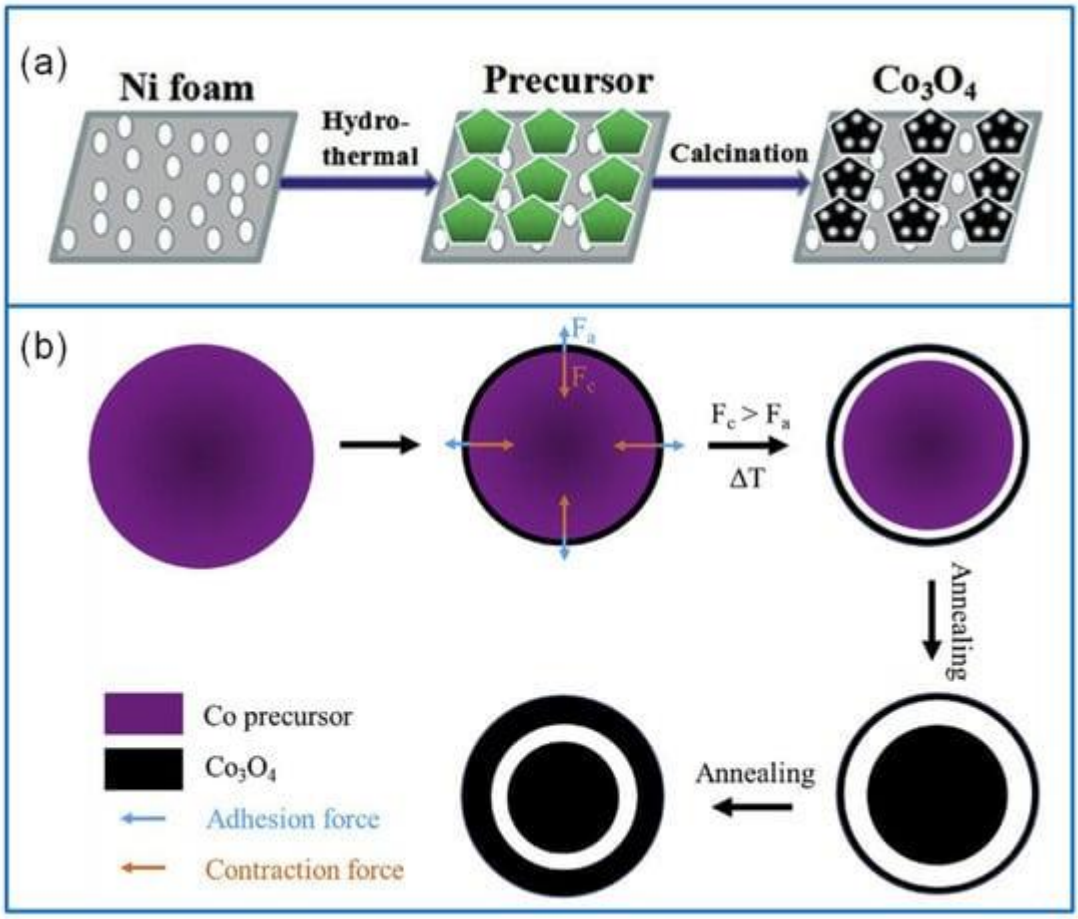

Figure 2-5. (a) Schematic diagram of preparing 2D ultrathin Co_3O_4 nanosheets (b) Schematic illustration of preparing core–shell Co_3O_4 mesoporous nanospheres using the solvothermal method [19]

2.4.3 Co-based composites

Experimental findings reveal that the energy storage performance of electrodes was considerably improved by the cooperative contributions of nanotubes (CNTs), graphene, and cobalt substitution. The composite with a 50% Co & 50% Ni ratio that is named $Co_{0.5}Ni_{0.5}(OH)_2$ displayed a remarkable specific capacitance of 2360 F g^{-1} at 360 mA h g^{-1} at current density of 0.5 A g^{-1} and sustained a high specific capacitance of 2030 F g^{-1} at 20 A g^{-1} with ~86% retention. The double hydroxides were able to modulate their redox

behavior, which was influenced by the ratio between cobalt and nickel. These findings demonstrate the significance of functional composites' rational design and large-scale assembly strategies in producing energy storage applications' enhanced performance and adjustability [20].

A two-step hydrothermal technique was utilized to prepare composite materials based on nickel-cobalt chalcogenides. The effect of adding 2D reduced graphene oxide sheets and replacing the anion with selenium on the morphology and crystalline phase of the materials was investigated. The corresponding changes in physicochemical properties were also examined, and their relationship to the altered electrochemical properties was explored. The $NiCo_2Se_4$/RGO electrode exhibited the highest specific capacitance of 1776 F g^{-1} at a 2 A g^{-1} and maintained excellent specific capacitance (51%) even at high current densities of 50 A g^{-1}. It is used to build a hybrid supercapacitor (HSC), the device gave a high specific capacitance of magnitude 212 F g^{-1} at 2 A g^{-1} [21].

2.5 Metal–organic frameworks

The MOFs are multi-dimensional materials composed of metal centers connected by organic linkers. There may be several thousand square meters per gramme of surface area in some of these MOFs because of the development of void spaces within the coordination network of the organic molecules. They are, however, not widely used in electrochemical systems because of their non-conducting nature. We've already discussed the advantages of composite materials that combine both electrochemical and redox-active materials with conducting carbons. Fleker et al. synthesized MOF-activated carbon compositions to talk about nonconductive nature of MOFs, a result of the network's coordinating bonds. MOF nanoparticles in contact with activated carbon show an interesting EPR signal [22]. The MOF's Cu^{2+}/Cu^{+} redox couple increases the AC's double-layer capacitance by 30 percent. Yaghi et al. reported a comprehensive study on the growth of MOF on graphene sets. Zirconium-MOF showed an aerial capacitance of 5.09 μF/cm for over 10,000 charge/discharge cycles [23].

Better composite materials may be produced by using wet or dry nanofabrication techniques. As organic nanoparticle fabrication techniques have become more homogeneous and reproducible, they have transformed the pharmaceutical and medical industry. For complex composite materials, the rapid prototyping field opens up new

possibilities. Of course, each technique must be adapted to fabricate high surface area electrodes, which requires additional development. The high surface area with porosity of MOFs provide numerous active sites for redox reactions, making them ideal for use in supercapacitor electrodes. Additionally, the structure and chemical composition of MOFs can be tailored to enhance their electrochemical properties, namely specific capacitance, energy density, and cycling stability. Overall, MOFs hold promise as a new class of electrode materials for supercapacitor devices, and ongoing research efforts are aimed at further optimizing their electrochemical performance for practical energy storage applications.

Summary

This chapter provides a summary of the properties and characteristics of suitable electrode materials for supercapacitor devices, such as activated carbon, carbon nanotubes, polypyrrole (PPY), graphene, polyaniline (PANI), and polythiophene (PTH). Overall, the literature review chapter provided insights into the latest research on electrode materials for supercapacitors and highlighted the need for further research in this area to develop high-performance energy storage devices with longer lifetimes, higher energy densities, and better power densities.

List of References

1. Verma, K.D., et al., *Characteristics of electrode materials for supercapacitors*, in *Handbook of Nanocomposite Supercapacitor Materials I: Characteristics*. 2020, Springer. p. 269-285.
2. Zhang, Y., et al., *Progress of electrochemical capacitor electrode materials: A review*. International journal of hydrogen energy, 2009. **34**(11): p. 4889-4899.
3. Sharmin, E. and F. Zafar, *Introductory chapter: metal organic frameworks (MOFs)*, in *Metal-organic frameworks*. 2016, IntechOpen.
4. Kolathodi, M.S. and T.S. Natarajan, *Development of high-performance flexible solid state supercapacitor based on activated carbon and electrospun TiO2 nanofibers.* Scripta Materialia, 2015. **101**: p. 84-86.
5. Wang, Y., et al., *Enhanced specific capacitance by a new dual redox-active electrolyte in activated carbon-based supercapacitors.* Carbon, 2019. **143**: p. 300-308.
6. Ben, J., et al., *Fabrication and electrochemical performance of PVA/CNT/PANI flexible films as electrodes for supercapacitors.* Nanoscale Research Letters, 2020. **15**: p. 1-8.
7. Li, H., et al., *Enhanced electrochemical performance of CuCo2S4/carbon nanotubes composite as electrode material for supercapacitors.* Journal of colloid and interface science, 2019. **549**: p. 105-113.
8. Wu, P., et al., *A low-cost, self-standing NiCo2O4@ CNT/CNT multilayer electrode for flexible asymmetric solid-state supercapacitors.* Advanced Functional Materials, 2017. **27**(34): p. 1702160.
9. Ahmad, R., et al., *ZIF-67 derived nitrogen doped CNTs decorated with sulfur and Ni (OH) 2 as potential electrode material for high-performance supercapacitors.* Electrochimica Acta, 2020. **364**: p. 137147.
10. Hu, Y., et al., *Effects of nitrogen doping on supercapacitor performance of a mesoporous carbon electrode produced by a hydrothermal soft-templating process.* Journal of Materials Chemistry A, 2014. **2**(30): p. 11753-11758.
11. Ramadoss, A. and S.J. Kim, *Improved activity of a graphene–TiO2 hybrid electrode in an electrochemical supercapacitor.* Carbon, 2013. **63**: p. 434-445.

12. Borenstein, A., et al., *Carbon-based composite materials for supercapacitor electrodes: a review.* Journal of Materials Chemistry A, 2017. **5**(25): p. 12653-12672.
13. Hao, G.-P., et al., *Structurally designed synthesis of mechanically stable poly (benzoxazine-co-resol)-based porous carbon monoliths and their application as high-performance CO2 capture sorbents.* Journal of the American Chemical Society, 2011. **133**(29): p. 11378-11388.
14. Wang, R., et al., *Metal/metal oxide nanoparticles-composited porous carbon for high-performance supercapacitors.* Journal of Energy Storage, 2021. **38**: p. 102479.
15. Lu, X., et al., *Hydrogenated TiO2 nanotube arrays for supercapacitors.* Nano letters, 2012. **12**(3): p. 1690-1696.
16. Raj, C.C. and R. Prasanth, *advent of TiO2 nanotubes as supercapacitor electrode.* Journal of The Electrochemical Society, 2018. **165**(9): p. E345.
17. Song, Z., et al., *Hydrothermal synthesis and electrochemical performance of Co3O4/reduced graphene oxide nanosheet composites for supercapacitors.* Electrochimica Acta, 2013. **112**: p. 120-126.
18. Wang, X., et al., *Recent advance in Co3O4 and Co3O4-containing electrode materials for high-performance supercapacitors.* Molecules, 2020. **25**(2): p. 269.
19. Cheng, Y., et al., *Improving the performance of cobalt–nickel hydroxide-based self-supporting electrodes for supercapacitors using accumulative approaches.* Energy & Environmental Science, 2013. **6**(11): p. 3314-3321.
20. Ghosh, S., et al., *Investigation of electrochemical charge storage in nickel-cobalt-selenide/reduced graphene oxide composite electrode and its hybrid supercapacitor device.* Journal of Alloys and Compounds, 2020. **835**: p. 155432.
21. Ramadoss, A. and S.J. Kim, *Improved activity of a graphene–TiO2 hybrid electrode in an electrochemical supercapacitor.* Carbon, 2013. **63**: p. 434-445.
22. Kolathodi, M.S. and T.S. Natarajan, *Development of high-performance flexible solid state supercapacitor based on activated carbon and electrospun TiO2 nanofibers.* Scripta Materialia, 2015. **101**: p. 84-86.

23. Bao, W., et al., Fabrication and electrical double-layer capacitance performance of interconnected and independent titania nanotube array. Materials Research Innovations, 2021. 25(1): p. 8-15.

Chapter 3: Review on Experimentation and Characterization Methods

3.1 Synthesis Method

For the proper synthesis of the catalyst material in the lab, many methods have been devised. Among them, some methods require special equipment while others can be performed without them. Choice of the catalyst synthesis process to form required NPs mainly rests on the preferred size, suitable properties of the surface, and the kind of material that is concerned such as semiconductors, metals, polymers, ceramics, etc. These methods have been researched and improved to increase the yield of our catalyst, obtain better structural properties and purity. Some of these methods have been discussed below:

3.1.1 Solvothermal Synthesis

It is a technique used for making a range of materials like semiconductors, metals, polymers, and ceramics. The method involves a solvent at moderate low to high pressure (usually between 1atm and 10,000 atm) & a temperature (from 100 °C to 1000 °C) which helps precursors in interaction during synthesis. If the solvent used is water, then the process is known as the "hydrothermal process." The conditions of the hydrothermal synthesis process are usually kept at the temperature of water around 374 °C. This method can be performed to make a wide variety of geometries such as thin films, single crystals, bulk powders, and nanocrystals. In addition, the formation (rod (2D), sphere (3D), and wire (1D) of crystals are organized by the control of chemical of interest concentration, solvent supersaturation, and control on kinetic. It can be used to form stagnant and thermodynamically stable forms involving novel elements that are not easily constructed from other synthetic paths. This review will emphasize some recent advances including the solvothermal process and nanocrystalline because in the last decade 80% of the literature focused on nanocrystals [1].

3.1.1.1 Synthesis of ZIF-67

ZIF-67 is usually prepared using solvothermal method. Simple scheme is used to synthesize ZIF-8. Metal salt cobalt nitrate hexahydrate is mixed with methanol to form a

solution. Organic linker 2-methyleimidazole is separately mixed with methanol to form another solution. Ratio of metal salt and organic linker is varied according to the morphology requirement and application. After that both solutions are mixed at room temperature while stirring. After 30 minutes of stirring solution is placed for 24 hours aging. After aging is finished purple precipitate settles down. Precipitate is thoroughly washed with ethanol and deionized water. Collected precipitate is dried in vacuum oven at 60 ℃ for 12 hours. After vacuum drying, sample is grinded to collect fine powder.

3.1.2 Hydrothermal Synthesis

This method is used to synthesize materials that require special conditions for the synthesis. Also, this method helps control the structure, morphology, and other properties of the material. Metal oxides, halides, composites that require specific temperature as well as pressure are usually synthesized by this method. The nanoparticles obtained by this method have characteristic properties. This method normally requires the use of an autoclave device in which temperature and pressure can be simultaneously controlled. The main significance of this process is the ability to synthesize a wide number of NPs that have upgraded composition, size, structure, and chemistry of surface that is reasonably cheap.

3.1.3 Pyrolysis

During pyrolysis, organic matter is decomposed into no condensable gases, condensable liquids, and biochar or charcoal as a residual solid product in an inert environment without oxygen.

3.1.4 Carbonization

Carbonization is a thermal decomposition process that produces a carbonaceous residue (while simultaneously removing the distillate) from organic substances. Pyrolysis is the oldest direct method of producing liquids from coal. It involves heating coal and capturing volatilized liquids, leaving behind a hydrogen-depleted carbon residue. In addition to the small amount of liquid that is produced (less than 20 percent), the mixture of chemicals and water contamination makes for a poor product. While organic matter is decomposed at high temperatures and the distillate is removed at the same time, carbonization is

primarily used to produce a carbonaceous residue known as coke. Carbonization of ZIF is performed to covert ZIF in to nano porous carbon and carbon nano tubes.

3.2 Characterization Techniques

3.2.1 X-Ray Diffraction (XRD)

This is one of the most important and common material characterization technique which provides information about the morphology, components, and crystallite size of the material. It uses X-ray radiations that pass through the material at an angle to the source. The diffraction angle is calculated, and the intensity is recorded. At an angle how many radiations deflect from a specific plane on the material gives information regarding its structure morphology.

To find evidence about the configuration of X-ray diffraction (XRD) of crystalline materials depend on the double particle/wave nature of X-rays. Identification and characterization of materials centered on their X-ray form are the major uses of the procedure. When a monochromatic X-rays incident beam contacts an object material the first outcome that takes place is atoms within the target substance scatter those X-rays as shown in Figure 3.1. The spread X-rays undertake destructive and constructive interference in the substances having proper structure (i.e. crystalline), which is called diffraction. The X-rays diffraction by crystals is told by Bragg‟s Law,

$$n(\lambda) = 2d\ Sin(\theta) \qquad (2)$$

The shape and size of the materials unit cell determine directions of likely diffractions. The atom's arrangement in the crystal structure affects the diffracted wave intensities. Many materials are not one crystal rather are comprised of little, small crystallites in all likely directions which are called polycrystalline powder or aggregate. A material with casually focused crystallites is put in an X-ray, the beam will view all available interatomic planes. When the experimental angle is scientifically altered, then all the available diffraction peaks from the substance will be identified [2].

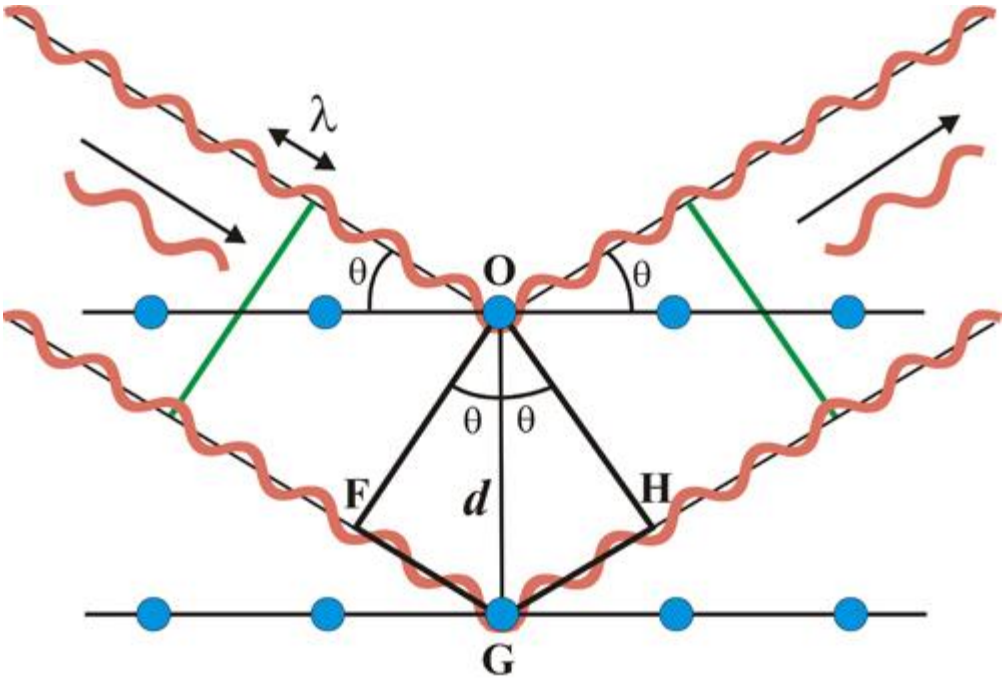

Figure 3-1. The Bragg's Law [1]

3.2.2 Scanning Electron Microscopy

The scanning electron microscope (SEM) makes use of a high-energy electrons-focused ray to produce a wide range of signals at the solid surface of the specimen. The high-energy electrons penetrate through the material and escape through the other end as shown in Figure 3.2. The information of the substance like chemical composition, crystalline structure, external morphology (texture), and materials orientation will be revealed signals of the electron beam and sample interactions. In various applications, a 2-dimensional image is formed that shows spatial variations in the properties, and numbers are collected over a particular choice area of the sample surface. The scanning method by simple SEM practices (magnification varying from 20X to around 30,000X, 3-D resolution of 50 to 100 nm) can be used to distinguish the areas that vary in size from about 1 cm to 5 microns in breadth. This method is exclusively valuable in semi quantitatively or qualitatively identifying chemical contents (by EDS), crystal orientations (using EBSD), and crystalline structure. The SEM is proficient in executing analyses of a specific area or point locations on the sample object. Its design and function are quite comparable to the EPMA and significant connections in abilities remain between the two devices [3].

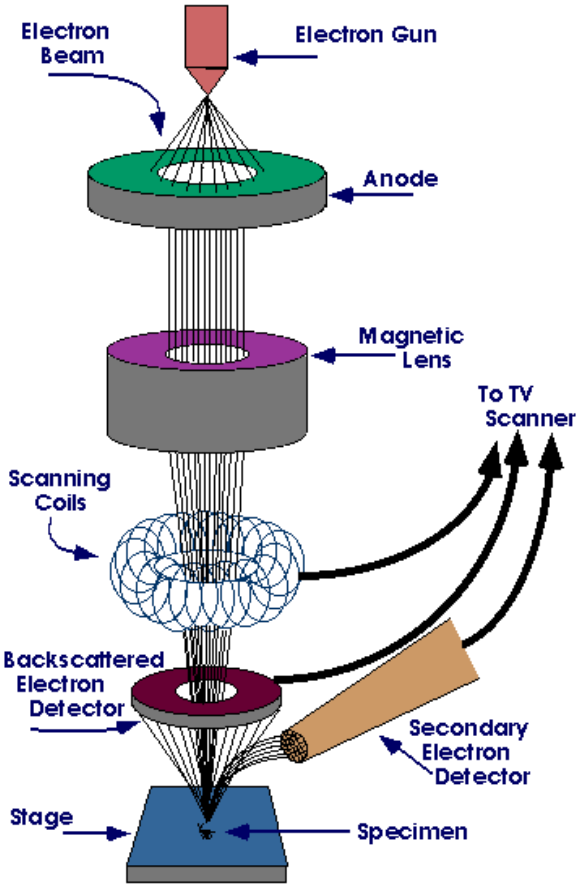

Figure 3-2. Illustration of how SEM works [2].

3.2.3 Energy Dispersive X-ray Spectroscopy (EDX)

EDS is one of a best elemental analysis method used to quantify the number of individual elements present in a nanoparticle. This technique gives the number of substances at a particular point but does not give the overall quantity of each element. It is usually combined with SEM or TEM to get a nanoscale image of particles through them, and EDS performs the analysis of that nanostructure. In the early 1970s, EDS developed into one commercial product and rapidly crossed WDS in popularity. The overall structure of the EDS is very simple because of no moving parts like the rotation detector in WDS. The sensor gathers the X-rays energies signal from all series elements in a sample at a similar time as compared to gathering signals from X-ray wavelength one by one which makes the EDS systems relatively fast as seen in Figure 3.3. The characteristic energy dispersion resolution is around 150–200 eV, which is lower than WDS resolve. The lightest

component that can be identified is not C (Z=6) rather O (Z=8). But major benefits like low cost and fast analysis make these disadvantages insignificant [2].

EDS band is a graph between the power of X-rays and the corresponding energies. Both light and heavy elements can be seen in a range of spectrum from 0.1 to 10-20 keV because both M or L lines of heavy elements and K lines of light elements are evident in this array.

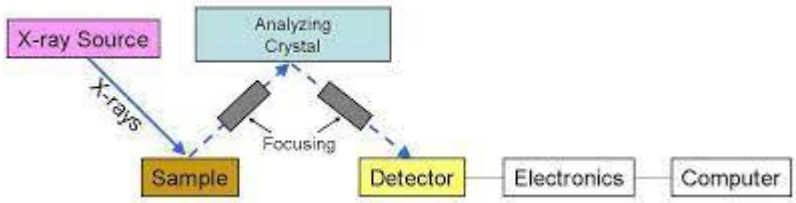

Figure 3-3. Illustration of EDX [3].

3.2.4 Thermo-Gravimetric Analysis

Thermogravimetric analysis (TGA) determines weight losses in a material with a change in temperature in a controlled atmosphere. The major applications of this characterization technique are the measurement of thermal stability, volatile content, moisture, organic linker in a sample, and the percent composition of components in a compound. The principle is that the temperature is gradually increased from zero to the required final temperature in a specific gas atmosphere which maybe Ar, air or some other gas. Now when temperature increases the contents in the sample start to evaporate. Moisture is usually the first content that removes from the sample so a change in mass of sample occurs. This mass is measured on the weight balance continuously during the process which is placed outside the furnace Figure 3.4. After moisture other volatile contents like organic residues start to escape. The stability of the sample can be defined as the temperature at which the material starts to decompose which is the main point in the curve. After that the line drops sharply causing a major loss in material. This point is called the decomposition temperature and determines the stability of material. The weight of the material is mapped against temperature to demonstrate the thermal changes in the sample, for instance, the loss of solvent, loss of water of hydration, and the decomposition of the material. At the end of the process, the final mass residue is noted, and the total mass loss is calculated [4].

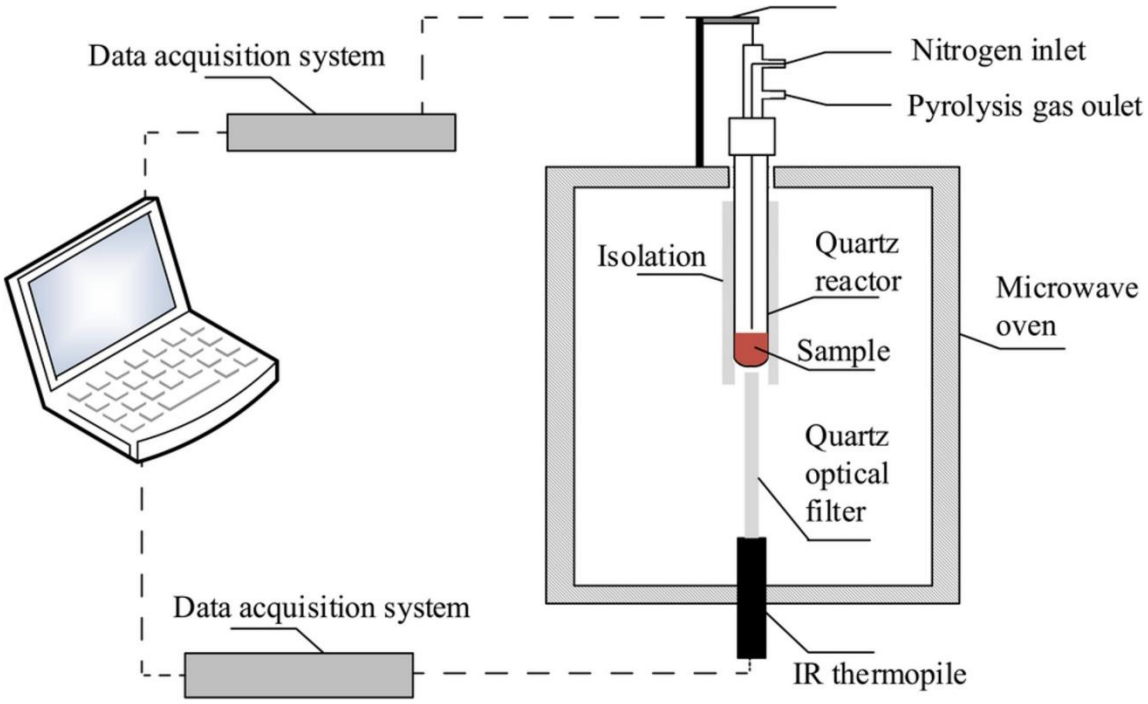

Figure 3-4. Schematic of TGA [4].

3.2.5 X-ray Photoelectron Spectroscopy

X-ray photoelectron spectroscopy (XPS) is known as a surface technique used to determine the chemical composition of a material. XPS works by irradiating a sample surface with a beam of X-rays, which causes the ejection of electrons from the surface atoms. The ejected electrons, called photoelectrons, are then collected and analyzed based on their kinetic energy and the angles at which they are detected. In XPS, the energy of the X-ray beam is typically set to a value greater than the binding energy of the electrons in the sample's outermost energy level, or valence band. When an X-ray photon with sufficient energy is absorbed by an atom, it can cause an electron from the valence band to be ejected, leaving behind a positively charged ion. The ejected photoelectron will carry information about the electronic structure of the atom it came from, including the chemical composition and bonding environment.

The kinetic energy of the ejected photoelectrons is measured using an electron analyzer, which separates the photoelectrons based on their kinetic energy and direction of emission. This technique can be used to identify the elements present in a sample, as well as the oxidation state and chemical environment of those elements. It is a highly sensitive technique, capable of detecting even trace amounts of impurities or surface contaminants.

XPS is widely used in materials science, surface chemistry, and semiconductor research to characterize the surfaces of materials, including metals, semiconductors, and polymers.

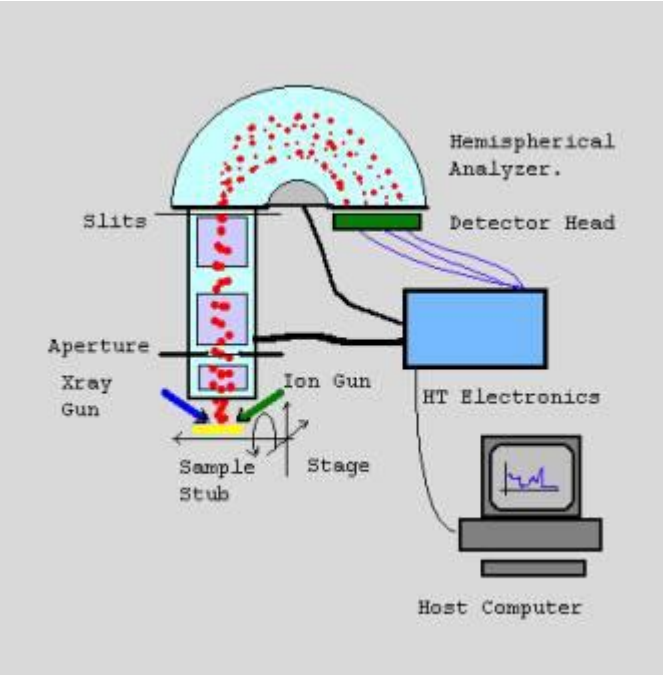

Figure 3-5. Schematic of XPS [4]

3.2.6 Transmission Electron Microscopy (TEM)

TEM is an imaging technique that allows for high-resolution imaging of materials at the nanoscale. The technique involves passing an electron beam through a sample, which interacts with the electrons and creates an image based on the interaction. In a TEM, a beam of high electrons is generated by an electron gun and focused by a series of electromagnetic lenses onto a thin sample. As the electrons pass through the sample, some are scattered, absorbed, or transmitted based on the density and thickness of the material. The transmitted electrons are then focused by additional lenses onto a fluorescent screen or a digital camera, producing a highly magnified image of the sample. TEM allows for the visualization of the internal structure of materials at atomic-scale resolution, as well as the observation of defects, dislocations, and other structural features that are difficult to observe with other techniques [3].

3.3 Electrochemical Testing

3.3.1 Slurry/Ink Formation

There are many substrates available for using as working electrode for example Glassy carbon electrode, nickel foam and carbon cloth. For every substrate method of ink formation is different. For glassy carbon we use ethanol as solvent and nafion (5 wt.% ion solution in lower aliphatic alcohols) as binder. Purpose of binder is to bind the active electrode material so that it sticks to the electrode. For nickel foam and carbon cloth we use PVDF as binder and n-methylepropyrilidine (NMP) as solvent. Carbon black/graphite powder/super-p is also added to the slurry. PVDF binder causes resistance that ultimately mitigate the overall conductivity of the active material. Purpose of carbon black is to cope with the reduced activity of active material caused by the PVDF binder. After mixing the required recipe, solution is sonicated for 4 hours to make homogenous suspension.

3.4 Electrochemical Techniques

When glassy carbon electrode is fabricated, it is dried at 60 degrees Celsius for 30 minutes. After that electrochemical testing is performed. For super capacitors three techniques are performed in electrochemical workstation.

- Cyclic Voltammetry (CV)
- Chronopotentiometry
- Electrochemical Impedance Spectroscopy (EIS)

3.4.1 Cyclic Voltammetry

Cyclic voltammetry is a great and common technique of electrochemistry used to study the oxidation-reduction procedures of molecular species. It is helpful to study chemical reactions started by electron transfer, which comprises catalysis. This electrochemical technique involves the running of the workstation through a complete cycle. The potential range was input into the software which is applied across the two electrodes. Scan rate, sample interval, sensitivity was given for each run along with several segments. Two segments make one complete cycle. The cyclic voltammetry gives information of the

current changing with voltage as shown in Figure 3.6 [10]. For CV, beaker cell was used in three electrode system. Glassy carbon, platinum wire and Ag/AgCl was used [6].

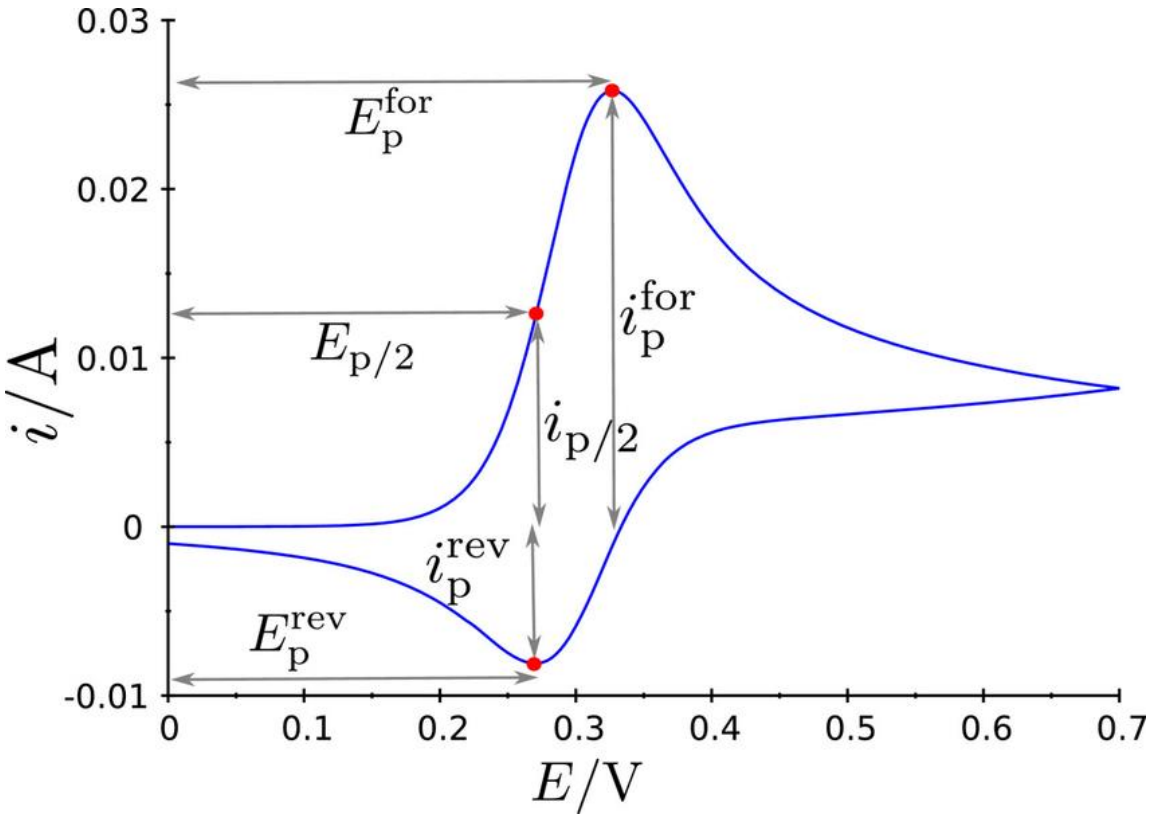

Figure 3-5. CV profile [7].

3.4.2 Chronopotentiometry

Chronopotentiometry is an electrochemical analysis method where the electrodes are subjected to a constant flow of current in order to the cause a constant reduction of the electroactive material Figure 3.7. This method is differentiated from constant-current coulometric analysis and coulometric titrimetry1 because in this technique the applied current appears to be significantly large so that the efficiency of current required for the reduction of the material is reduced below 100% within a few seconds.

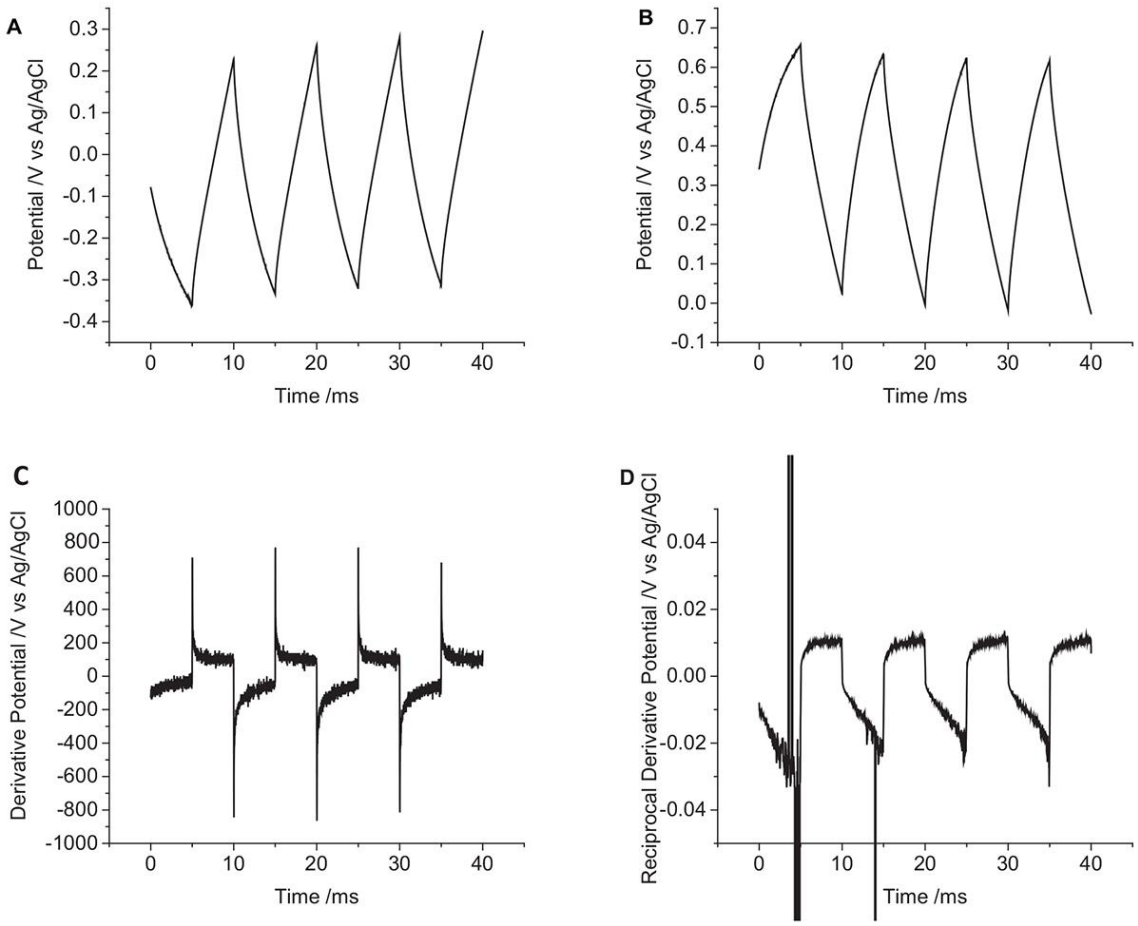

Figure 3-6. Chronopotentiometry Profile [8].

3.4.3 Electrochemical Impedance Spectroscopy (EIS)

This technique of electrochemical workstation allows us to measure the resistivity of our system. This includes resistance of electrolyte, ohmic loss and or activation losses. Electrical resistance is the measure of the of a circuit element that resists current flow.

$$R = E/I \quad (3)$$

According to Ohm's law, R is the resistance which is defined as the ratio of voltage (E), and current (I). This known law use is used to find only one circuit element, the ideal resistor.

- Ohm's Law is followed at every range of current and voltage.
- Resistance is not dependent on the frequency.
- The voltage passing through a resistor and the AC current are in a single phase.

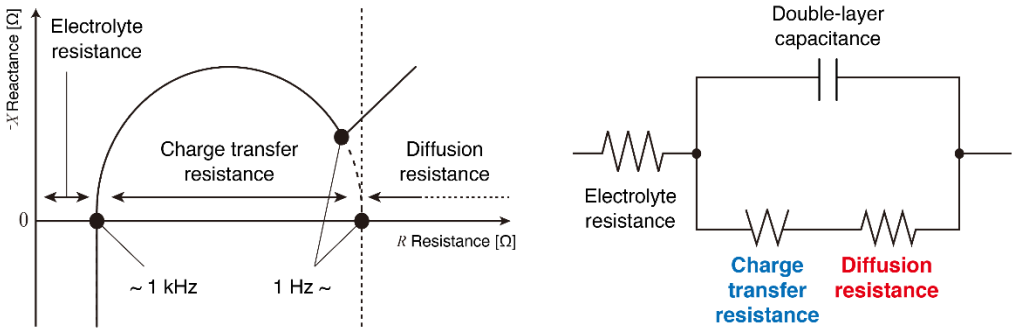

Figure 3-7. EIS Profile (Nyquist Plot) [9].

3.5 Electrochemical Parameters

The determination of the energy density along with power density is very important to evaluate the efficiency of a supercapacitor. Cyclic voltammetry (CV) and chronopotentiometry are the techniques that can confirm the energy and power densities by using the following equations:

The specific capacitance (F g^{-1}) can be determined using cyclic voltammetry:

$$C_s = \frac{\int \mathrm{IdV}}{2mv\Delta V} \tag{4}$$

Here, ∫IdV is the integral area of CV curves, m represents the mass, n represents the scan rate used to perform the analysis, and the voltage window of the process is represented by V.

$$E = \frac{1}{2}\frac{C_m \Delta V^2}{3.6} \tag{5}$$

Here, E is the symbol for energy density. The maximum specific power is calculated as:

$$P = \frac{E}{\Delta \mathrm{t}} \times 3600 \tag{6}$$

Here, P represents the maximum power that can be achieved by a supercapacitor.

Summary

This chapter initially discusses different chemical synthesis methods like solvothermal and hydrothermal method. After that material characterization techniques have been studied i.e., XRD, SEM, EDS, TGA, BET and XPS . Main principle of these techniques has been noted down along with diagrams. After that the whole electrochemical testing process implemented was explained including ink formation, ink deposition on substrate and electrochemical performance determination using various techniques like CV, CP, and EIS with a three-electrode system.

List of References

[1] T. Takahashi, K. Kuwabara, and M. Shibata, "Solid-state ionics - conductivities of Na+ ion conductors based on NASICON," *Solid State Ionics*, vol. 1, no. 3–4, pp. 163–175, 1980, doi: 10.1016/0167-2738(80)90001-6.

[2] N. S. Mohamed, R. H. Y. Subban, and R. Rusdi, "Enhancement of electrical properties of NASICON-type solid electrolytes (LiSn2P3O12) via aluminium substitution," *J. Sci. Adv. Mater. Devices*, vol. 5, no. 3, pp. 368–377, 2020, doi: 10.1016/j.jsamd.2020.06.003.

[3] F. Zheng, M. Kotobuki, S. Song, M. O. Lai, and L. Lu, "Review on solid electrolytes for all-solid-state lithium-ion batteries," *J. Power Sources*, vol. 389, no. April, pp. 198–213, 2018, doi: 10.1016/j.jpowsour.2018.04.022.

[4] C.J.Brinker;G.W.Scherer,"Sol-Gel_Science_The_physics_and_chemistry_of_sol-gel_processing_-_Brinker_1990.pdf." p. 462, 1990. doi: 10.1016/S0254-0584(02)00315-2.

[5] S. D. Lee *et al.*, "Composite Electrolyte for All-Solid-State Lithium Batteries: Low-Temperature Fabrication and Conductivity Enhancement," *ChemSusChem*, vol. 10, no. 10, pp. 2175–2181, 2017, doi: 10.1002/cssc.201700104.

[6] J. Lai, W. Niu, R. Luque, and G. Xu, "Solvothermal synthesis of metal nanocrystals and their applications," *Nano Today*, vol. 10, no. 2, pp. 240–267, 2015, doi: 10.1016/j.nantod.2015.03.001.

[7] X. Dong, M. Qi, Y. Tong, and F. Ye, "Solvothermal synthesis of single-crystalline hexagonal cobalt nanofibers with high coercivity," *Mater. Lett.*, vol. 128, pp. 39–41, 2014, doi: 10.1016/j.matlet.2014.04.133.

[8] S. Sōmiya and R. Roy, "Hydrothermal synthesis of fine oxide powders," *Bull. Mater. Sci.*, vol. 23, no. 6, pp. 453–460, 2000, doi: 10.1007/BF02903883.

[9] S. Feng and R. Xu, "New materials in hydrothermal synthesis," *Acc. Chem. Res.*, vol. 34, no. 3, pp. 239–247, 2001, doi: 10.1021/ar0000105.

Chapter 4: Methodology and Experimentation

4.1 Chemical Reagents

All the chemicals were purchased from the Sigma Aldrich with high purity. No further purification process was carried out for any chemical. Titanium tetra-n-butoxide ($Ti(C_4H_9O)_4$, reagent grade 97% pure), cobalt (II) nitrate hexahydrate ($Co(NO_3)_2.6H_2O$, purity >99%), and 2-Methylimidazole ($C_4H_6N_2$, MeIM, purity >99%) were used in this synthesis process. Deionized water (DI) and ethanol were used as solvents.

4.2 Material Synthesis

4.2.1 Synthesis of ZIF-67

A simple co-precipitation method was used in this step to obtain ZIF-67 as basic precursor. Two solutions were stirred and prepared separately. The first solution was made by dissolving 1 mmol cobalt nitrate hexahydrate in 50 ml DI water while second solution contained 8 mmol of 2-MeIM dissolved in 50 ml DI water. Both solutions were stirred for 30 minutes at room temperature till the formation of clear solutions. The first solution was then poured into second while stirring vigorously to get purple solution. It was then kept stirring for 24 hours followed by 24 hour aging. The solution was filtered and washed several times with DI water and ethanol to remove any unreacted species or impurities. Filtrate was dried at 80 ℃ under vacuum. Dried precipitates were ground into fine powder in mortar pestle.

4.2.2 Carbonization of ZIF-67 to Co/NGC

Fine purple powder was pyrolyzed in reducing environment (H_2/Ar in 1:9 ratio) initially heated to a temperature of 350℃ and kept for 1.5 hours to completely convert the ZIF-67 structure into nano graphitic carbon (NGC). Then, at 700 ℃, 800 ℃ and 900 ℃ with a heating rate of 5 ℃/minute and a stay time of 3.5 hours was provided for complete conversion of metal species into metallic cobalt. The obtained black powder was again ground into fine powder before any further treatment. Obtained samples were named as Co@700, Co@800, and Co@900 respectively.

4.2.3 Solvothermal Synthesis of Titania/Cobalt Composite

Firstly, a solution containing 1.5 ml titanium tetra-n-butoxide and isopropanol was prepared using sonication of at least 1 hour. Further, 1 g of pyrolyzed sample was added to this solution and sonicated for 1 hour. The mixture was shifted to a 100 ml Teflon-lined autoclave. It was heated to 160 ℃ and kept for 24 hours to obtain titania-based composite of ZIF-67 derived Co-NGC. The greenish colored filtrate was then dried at 70 ℃ for 12 hours. Obtained material was ground into fine powder for further characterizations and testing. Same steps were repeated for all samples. Obtained samples are named as TZ-700, TZ-800, and TZ-900 respectively.

4.3 Material Characterization

Powder X-ray diffraction technique is used to determine phase crystallinity of the prepared samples, Cu–Kα rays were used in XRD (Bruker D8-Advance) measurement. Peaks of the as synthesized materials were studied at a scan of 0° to 70^0. To investigate the morphology of particles, scanning electron microscopy, SEM (SEM, NovaSEM, FEI) was used. X-ray photoelectron spectroscopy (XPS, Thermo Fisher Scientific ESCALAB 200i) was carried out to evaluate the chemical bonding in prepared samples. XPS survey spectra was obtained along with elemental composition. Transmission Electron Microscopy (TEM, Tecnai G^2 F29, FEI)) analysis were performed to get high resolution images of prepared composites. To identify the mass loss with increasing temperature, thermo-gravimetric analysis was performed on Discovery TGA 5500 in nitrogen atmosphere.

4.4 Electrochemical Measurements

Electrochemical workstation 660E by the CH instruments was implied to execute the electrochemical testing of the prepared electrodes. Cyclic voltammetry (CV), gravimetric charge-discharge (GCD), along with electrochemical impedance spectroscopy (EIS) were carried out in three electrode configurations. In this three-electrode system, Ag/AgCl was used as reference electrode, with platinum wire as counter electrode, and glassy carbon was used as current collector. 1M KOH, 1 M Na_2SO_4 and 1 M H_2SO_4 were used as aqueous electrolytes for the testing. The slurry was prepare by adding 2 mg active material, 20 µl binder (Nafion perfluorinated resin solution, 5%), and 80 µl ethanol, after mixing this mixture was sonicated for 30 minutes to obtain a homogeneous slurry. A drop

of 1.5 µl was casted on glassy carbon with the help of micropipette and dried for 5-10 minutes at room temperature to make working electrode. The potential window of -0.15V – 0.5V was selected to perform electrochemical testing for all the electrolytes.

Summary

This chapter includes the total experimentation that was involved in the research process. The synthesis process of ZIF-67, carbonization of ZIF-67 based nitrogen doped carbon and conversion to titania based quaternary composites along with their characterization techniques used were thoroughly demonstrated in the chapter. Finally, the electrochemical testing techniques which were used on electrochemical workstation and the testing parameters are discussed.

List of References

[1] W. Yang, X. Shi, Y. Li, H. Pang, Manganese-doped cobalt zeolitic imidazolate framework with highly enhanced performance for supercapacitor, J. Energy Storage. 26 (2019) 1–7. https://doi.org/10.1016/j.est.2019.101018.

Chapter 5: Results and Discussion

5.1 Material Characterization

5.1.1 X-ray Diffraction (XRD)

Figure 5.1(a) shows the XRD pattern of prepared samples TZ-700, TZ-800, and TZ-900 while XRD patterns after ZIF-67 pyrolysis in comparison with titania incorporated samples is shown in S1. After ZIF-67 pyrolysis at 700 ℃, 800 ℃, and 900 ℃, the obtained XRD pattern indicates the presence of metallic cobalt with reference to JCPDS # 15-0806 as shown in S1. The diffraction peaks near 26° indicates the presence of carbon [1]. During the solvothermal reaction for incorporation of titania, some of the metallic cobalt is converted to cobalt oxide (Co_3O_4) whose peak can be indexed at 36.5^0 with the plane (220) as seen from figure 5.1(a). Also, the peak intensity of Co_3O_4 increases as we move from TZ-700 to TZ-900 showing the enhanced crystallinity. Relative intensity of metallic cobalt is reduced after solvothermal reaction as it converts to cobalt oxide (Co_3O_4). TiO_2 presence in prepared samples can be well matched with JCPDS # 21-1272 corresponding to 2θ values of 25.2°, 48.0°, 62.1°, 70.3°, 75.0° and 76.0° allocated to the (1 0 1), (2 0 0), (213), (220), (215) and (301) planes. To confirm the presence of carbon in titania incorporated samples, Raman spectroscopy is performed. Degree of graphitized carbon could also be confirmed through calculation of I_D/I_G. Figure 5.1(b) shows the Raman spectrum of prepared samples having two prominent bands namely D (disorder induced) and G (graphitic) bands. D and G bands are present at around 1350 cm^{-1} and 1580 cm^{-1} [2]. I_D/I_G as calculated from the data are 1.21, 1.09, and 0.822 for TZ-700, TZ-800 and TZ-900 respectively. It shows higher degree of graphitization in the sample prepared at 900^0C. Higher degree of graphitic carbon improves the electrical conductivity that is one of the reasons behind highest specific capacitance of TZ-900 [3, 4].

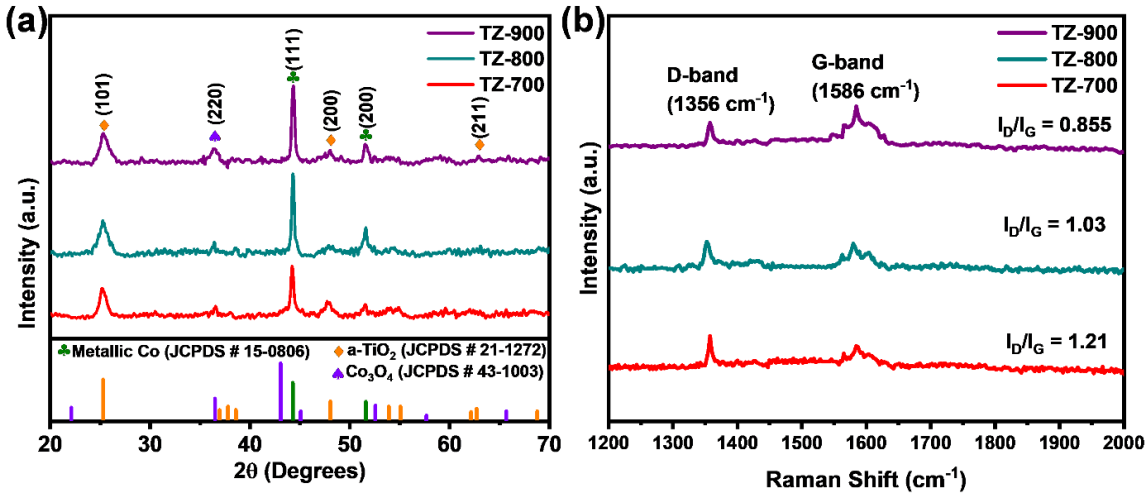

Figure 5-1. (a) XRD pattern (b) Raman Spectra of TZ-700, TZ-800, and TZ-900

5.1.2 Scanning Electron Microscopy (SEM)

The electron micrograph acquired from pyrolyzed substances depict numerous agglomerations of particles and suggests that this fabric consists of particles with one of a kind particle measurement except any described geometrical shapes as shown in Figure 5.2. It is evident from the literature that with increasing carbonization temperature, the particle size of ZIF-67 is increased [34, 44]. Therefore, the prepared samples show a higher particle size when formed composite with titania. TZ-700 shows an agglomerated morphology showing the dispersion of titania over surface of ZIF-67 structure that was decomposed during carbonization. TZ-800 Figure 5.2 (b,e) and TZ-900 in Figure 5.2 (c,f) images show a greater agglomeration and disrupted structure as compared to TZ-700. The average particle size distribution was found to increase from 52 nm to 69 nm as calculated by averaging 10 to 20 particles using the software ImageJ. It has also increased the surface coverage of the particles with titania that can be predicted as the reason for increased electrochemical properties i.e., electric double layer phenomenon. The introduction of titania has converted the morphology of ZIF-67 to spherical particles which can be seen clearly in the sample TZ-900 [45]. An increase in roughness of particles' surface is seen in Figure 5.2 (f) with increasing carbonization temperature that too, is supported by literature [46].

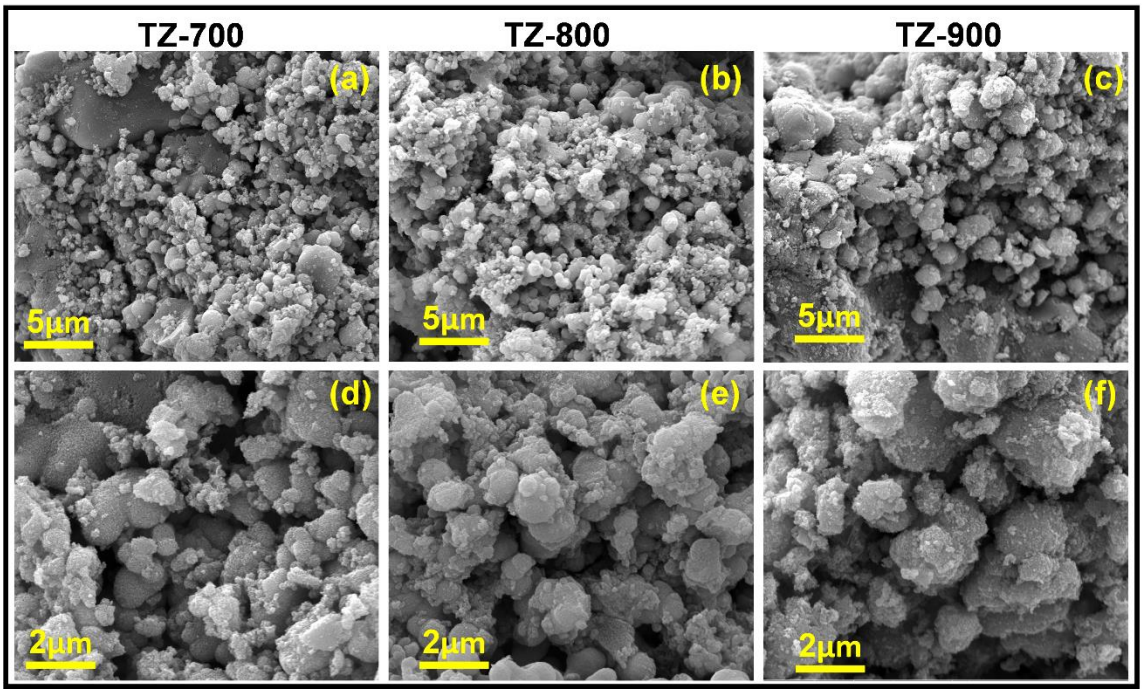

Figure 5-2. SEM images of (a,d) TZ-700, (b,e) TZ-800 and (c, f) TZ-900

5.1.3 Transmission Electron Microscopy

Figure 5 shows the TEM and HRTEM images along with EDX of the sample TZ-900. A nearly globular morphology can be seen in figure 5.3 (a) that is in line with the SEM images presented before. Also, the uniform distribution of titania over the surface of Co-C species depicts better surface activity. It can be seen in HRTEM (Fig 5.3 (b)) that there is a sharp plane corresponding to titania in anatase phase with a d-spacing of 3.52 nm for the plane (102). A live profiling of a-TiO_2 is shown in Figure 5.3 (d). The intensity of this plane is highest as seen in the XRD spectrum of this sample. It shows the increased crystallinity of the prepared sample. Also, metallic cobalt planes can be located adjacent to a-TiO_2 with a d-spacing of 2.05 nm corresponding to the plane (111) in Figure 5.3 (b) which is also evident from the XRD pattern. (220) plane of Co_3O_4 is marked with a d-spacing of 0.285 nm that is matched with the JCPDS card no. 43-1003. Moreover, there are inter-linked and overlapping planes of titania and cobalt that can present a synergistic relation between Ti^{+4}, Co^{+3} and metallic cobalt resulting in better charge transfer and hence, the electrochemical activity [5, 6]. EDX analysis of TZ-900 is presented in Figure 5.3 (c). EDX mapping is shown in the Figure 5.3 (e-i) that shows a uniform distribution of titania and other elements in the sample TZ-900.

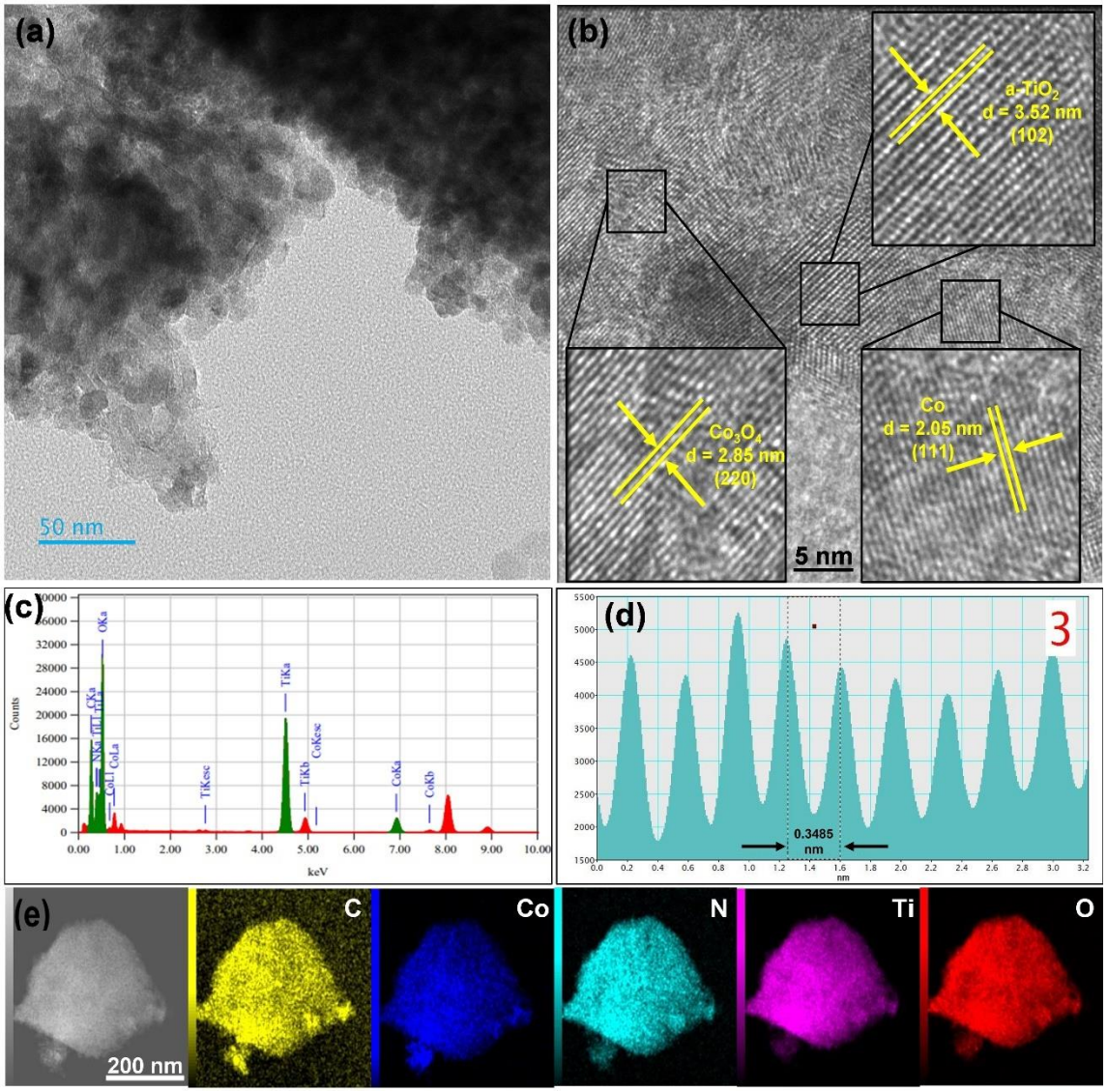

Figure 5-3 (a)TEM image at 50 nm (b)HRTEM image showing planes of a-TiO_2, metallic Co, and Co_3O_4 (c) EDX elemental composition (d) Live profile showing a-TiO_2 (e) EDX mapping

5.1.4 X-ray photoelectron spectroscopy

XPS was performed to examine the surface composition and chemical state. The XPS survey spectrum of the TZ-700, TZ-800 and TZ-900 is shown in Figure 5.4 (a). The percentage of carbon species increases with temperature while the metals proportion is lessened. XPS quantitative analysis is presented in table 1 that confirms the variation in Co, Ti, C, N, and O percentage. Figure 5.4 (b-f) shows the deconvoluted spectrum of TZ-

900. Figure 5.4 (b) shows the deconvolution of Co 2p spectrum that confirmed the presence of metallic cobalt, cobalt (III) oxide and cobalt (II) oxide with the peaks located at 778.5 eV, 780.2 eV, 796.6 eV, 781.9 eV, and 796.9 eV for Co^{0} ($2p_{1/2}$), Co^{+3} ($2p_{1/2}$), Co^{+2} ($2p_{1/2}$), Co^{+3} ($2p_{3/2}$), and Co^{+2} ($2p_{3/2}$) respectively [7-10]. Mix metal oxidation states can be used to store and transfer electrical charge in materials. These states occur when an atom or molecule has more than one oxidation state, or valence, in each compound. The ability of a molecule to exist in multiple valence states allows for greater flexibility in the transfer of electrons, which can be used to generate or store electrical charge [9]. Figure 5.4 (c) presents the deconvoluted peaks for Ti 2p. Ti 2p spectrum shows the two prominent bands at 459.2 eV and 465.1 eV corresponding to Ti $2p_{1/2}$ & Ti $2p_{3/2}$ where Ti exists in Ti^{+4} state [11]. Figure 5.4 (d) shows deconvoluted spectrum of C 1s. Peaks at 284.5 eV, 285.1 eV, 286.4 eV, and 288.1 eV are attributed to the presence of C-C, C-N, N-C=O, and O-C=O respectively [12]. Figure 5.4 (e) shows the deconvoluted peaks of O 1s confirming the presence of metal oxides at the peak position 530.3 eV [13]. Figure 5.4 (f) is the deconvolution of N 1s spectrum showing the presence of pyridinic N, Co-N, graphitic and pyrrolic N at the peak position of 398.6 eV, 399.5 eV, 400.2 eV, & 401.3 eV [14].

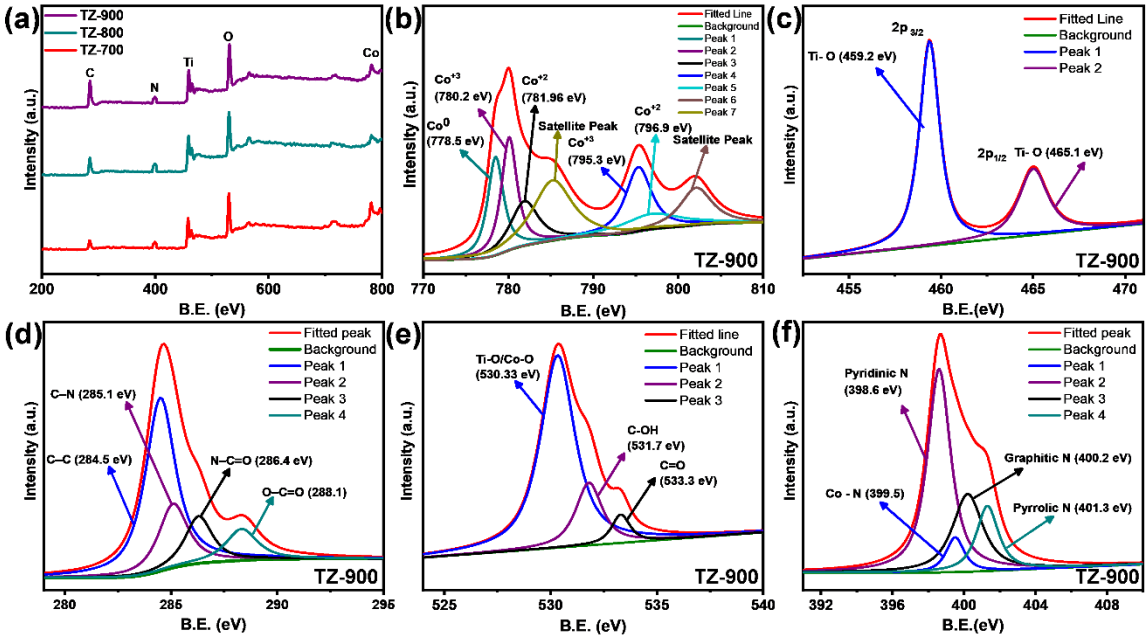

Figure 5-4 (a) XPS survey spectrum of TZ-700, TZ-800 and 900 showing the ratio of elements in the sample. The deconvoluted XPS spectra of (b) Co2p, (c) Ti2p, (d) C1s, (e) O1s, and (f) N1s.

Table 5. 1 The atomic percentage of elements present in samples.

Sample	C (%)	N (%)	O (%)	Ti (%)	Co (%)
TZ-700	26.39	0.71	50.16	12.57	10.17
TZ-800	37.30	2.00	42.42	13.75	4.53
TZ-900	48.36	0.59	37.14	9.19	4.72

5.1.5Thermogravimetric Analysis

TGA curve of ZIF-67 was recorded before the incorporation of TiO_2 in the structure as shown in figure 5.5. It shows that major mass loss can be seen in the temperature of 300 to 400 ℃. It indicates the stability of ZIF-67 up to 300 ℃ after which the conversion to carbon species starts. There is no indication of mass loss from 700 to 800 ℃ but a loss of further 4% above this temperature. A mass loss of 12% is observed up to 300 ℃ followed by a rapid mass loss of 66% that is the property of carbon-based materials owing to the removal of CO, CO_2, and other alkyl groups. It occurs due to thermal degradation of methylimidazole linker at temperatures higher than 450 ℃. After 800 ℃, there is very little mass loss that shows the presence of metals that do not lose its mass on high temperatures [15, 16]. A further mass loss of 4% after 800 ℃ can be seen for sample TZ-900.

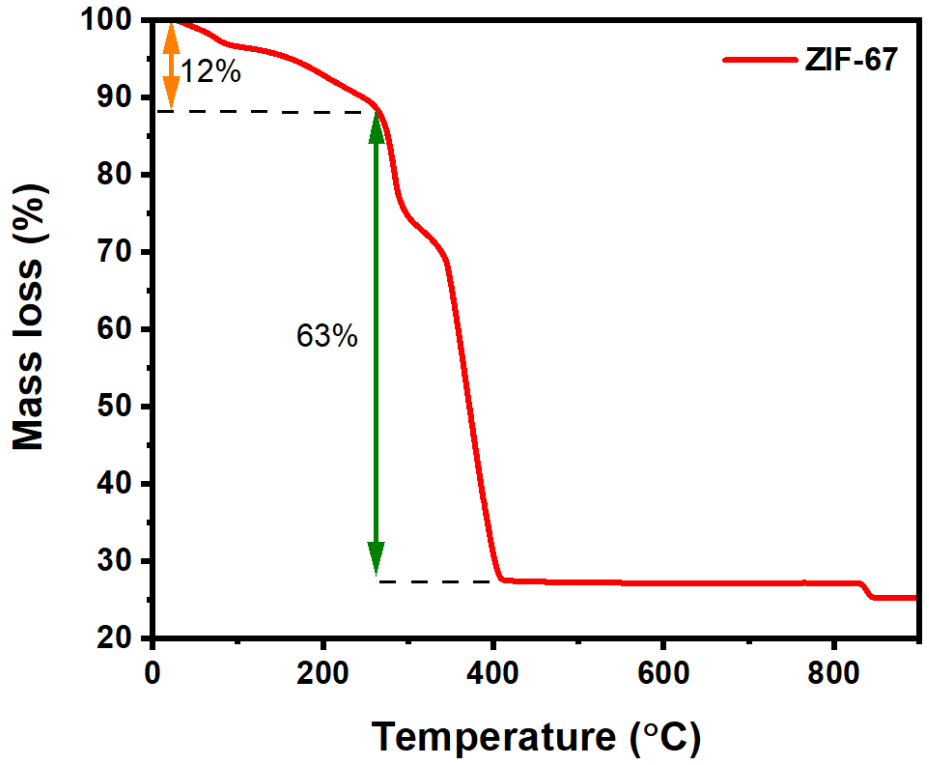

Figure 5-5. TGA profiles of ZIF-67.

5.2 Electrochemical Performance

The electrochemical performance evaluation was done using CV, GCD, and EIS in a 3-electrode configuration.

5.2.1 Cyclic Voltammetry (CV)

To evaluate the electrochemical parameters of electrode materials (TZ-700, TZ-800, and TZ-900), CV, GCD, and EIS measurements were conducted. All the above-mentioned formulas were used in this section to calculate the specific capacitance through these curves.

Figure 8 shows the CV curves of prepared electrodes in three electrolytes (a) 1M KOH, (b) 1M H_2SO_4 and (c) 1M Na_2SO_4 at a scan rate of 40 mV s^{-1}. CV curves in alkaline electrolyte i.e., 1M KOH as shown in Figure 5.6 (a) present a pseudocapacitive behaviour having highest current density in TZ-900 followed by TZ-800 and TZ-700. It shows an increase in specific capacitance for the electrode, TZ-900. There are slight redox peaks showing the oxidation and reduction of Co present in the electrode material. For the acidic electrolyte i.e., 1M H_2SO_4 as shown in Figure 5.6 (b), shape of CV curve is nearly a

rectangle showing the electric double layer capacitor (EDLC) behaviour. A highest area enclosed in the CV curve of TZ-900 is obtained showing a highest specific capacitance as presented later by GCD calculations. In the neutral electrolyte i.e., 1M Na_2SO_4 as shown in Figure 5.6 (c) an EDLC behaviour is observed but less rectangular as compared to that of acidic electrolyte. It can be concluded that specific capacitance is dependent on the type of electrolyte used. Figure 5.6 (d) shows the comparison of specific capacitance as calculated from the CV curves at 40 mV s^{-1}.

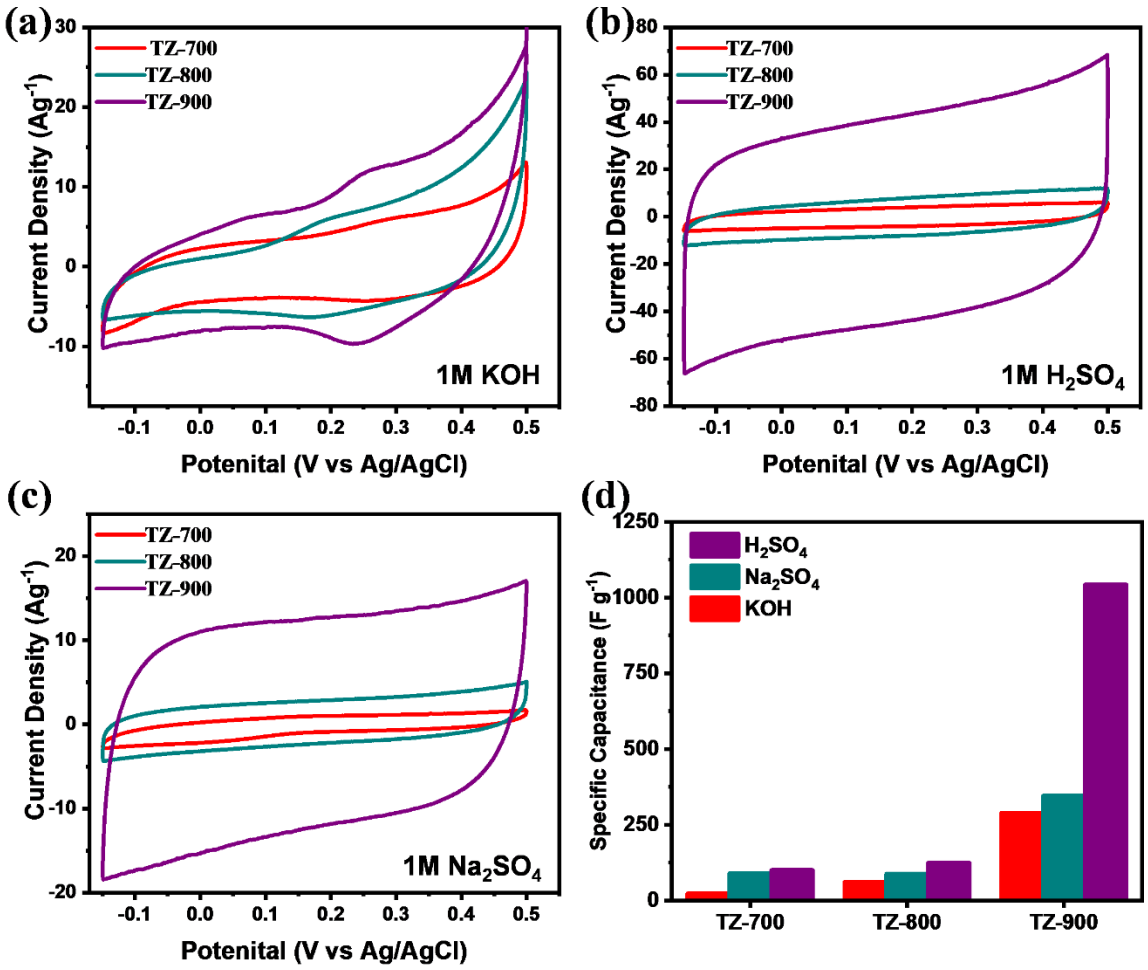

Figure 5-5. CV curves comparison at scan rates 40 mV s^{-1} of TZ-700, TZ-800, and TZ-900 in (a) 1M KOH, (b) 1M H_2SO_4, (c) 1M Na_2SO_4, (d) Calculated specific capacitance of electrodes at 40 mV s^{-1}.

5.2.2 Chronopotentiometry

Figure 9 presents the charge/discharge profiles of electrode materials. Figure 5.7 (a) presents a comparison of GCD profiles of prepared samples in KOH electrolyte showing the specific capacitance of 183.77, 214.21, and 221.75 F g^{-1} for TZ-700, TZ-800, and TZ-900 respectively at 0.5 A g^{-1}. Figure 5.7 (b) is the comparison of GCD profiles in H_2SO_4 showing the specific capacitance of 303.02, 644.95, and 1617.5 Fg^{-1} for TZ-700, TZ-800, and TZ-900 respectively at 0.5 A g^{-1}. In Na_2SO_4, as presented in figure 5.7 (c), the specific capacitance is calculated to be 198.6, 240.3, and 269.81 F g^{-1} for TZ-700, TZ-800, and TZ-900 respectively 0.5 A g^{-1}. Figure 5.7 (d) presents the comparison of specific capacitance values in acidic, basic, and neutral electrolyte for TZ-700, TZ-800, and TZ-900 at 0.5 A g^{-1}. The specific capacitance is highest in the acidic electrolyte for all the prepared. It is due to difference in ionic radii, ionic conductivity, and ionic mobility. The hydrated radius of K^+, H^+, and Na^+ in the electrolytes KOH, H_2SO_4 and Na_2SO_4 are 0.331 nm, 0.28 nm, and 35.8 nm respectively. Moreover, the molar ionic conductivity of K^+ in KOH is 73.5 S cm^2 mol^{-1}, H^+ in H_2SO_4 is 350.1 S cm^2 mol^{-1} and Na^+ in Na_2SO_4 is 50.11 S cm^2 mol^{-1} [20]. Due to lower hydrated ionic radius of H^+ and highest molar ionic conductivity, it can be assumed that prepared electrodes outperformed in acidic electrolyte. Due to increased mobility of H^+ ion owing to its smallest hydrated ion size that helps in the formation of EDLC layer, high specific capacitance is observed in sulfuric acid. Also, sulfuric acid presents low equivalent series resistance that in turn enhances the ionic conductivity leading to high specific capacitance [21, 22].

There is an increased specific capacitance with increasing temperature composite as TZ-900 has shown the higher specific capacitance than TZ-700 and TZ-800. The reason behind this increase is uniformity and higher surface coverage of carbonized structured with titania. This increased capacitance can be attributed to uniform distribution of TiO_2 species across the graphitic carbon matrix that prevent agglomeration as well as restacking of carbon species. It resulted in EDLC behaviour of the prepared sample with fast transfer of electrons due to titania in electrode matrix [23]. Energy density and power density is calculated from the specific capacitance at 0.5 A g^{-1} shown in table 5.2.

Table 5-2. Specific capacitance with energy density of all the synthesized samples at current density 5 A g^{-1}

Electrode Material	Specific Capacitance (F g^{-1})	Energy Density (Wh kg^{-1})
TZ-700	303.02	17.78
TZ-800	644.95	37.84
TZ-900	1617.5	94.91

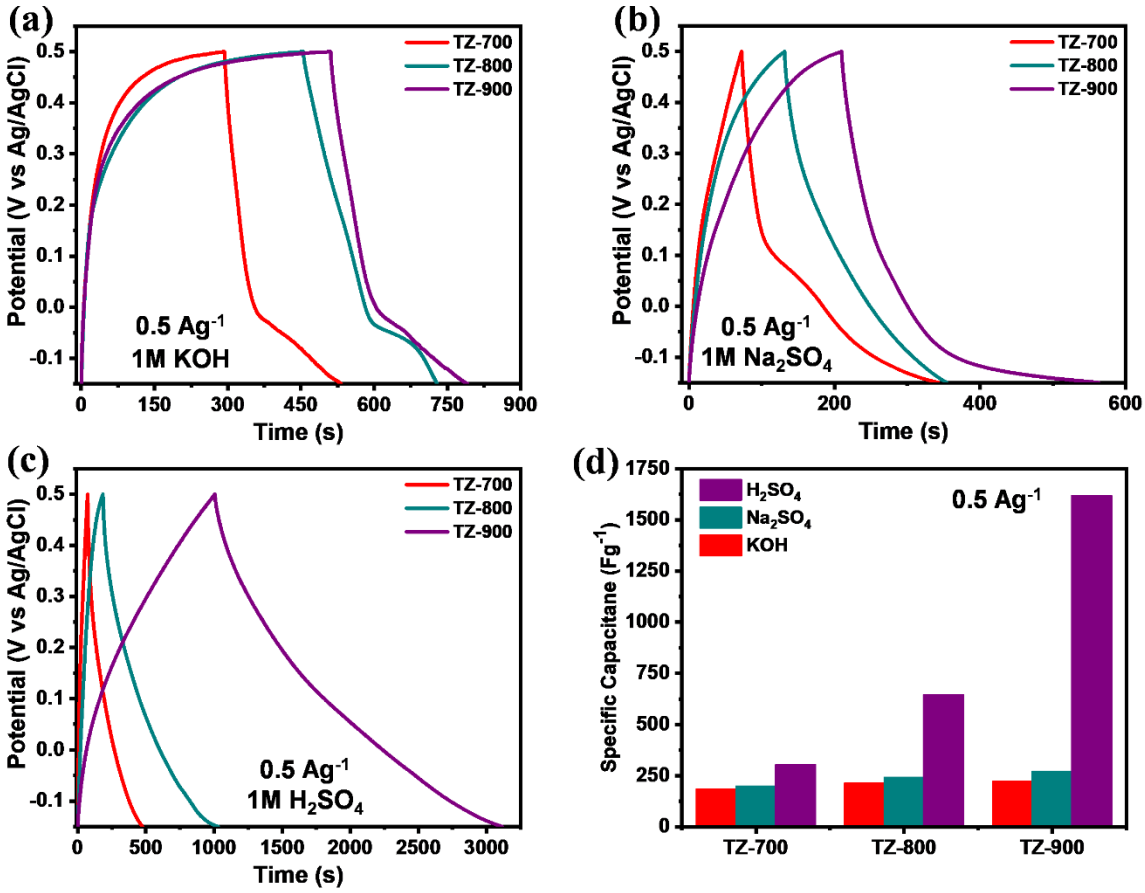

Figure 5-6. GCD curves at current densities of 0.5-2.5 A g^{-1} of TZ-700, TZ-800, and TZ-900 in (a) 1M KOH, (b) 1M H_2SO_4, (c) 1M Na_2SO_4, (d) Calculated specific capacitance of electrodes at 0.5 A g^{-1}.

5.2.3 Capacitive and Diffusive Contribution

A comprehensive mathematical analysis was carried out to gain a deeper insight into the material charge storage behavior. The electrode material's total specific capacitance can be split into two components based on the storage mechanism: EDLC and diffusion. EDLC is attributed to the surface adsorption and desorption of ions and is rapid and

unassociated with the scan rate. Diffused control is dependent on the electrolyte ions' diffusion into the electrode material's surface. To reach conclusive outcomes, it is essential to determine which process dominates during an electrochemical reaction. For such a linear scan rate, the current is given by Equation 5.

$$i = av^b \tag{5}$$

Rearranging Equation 1 as:

$$i(V) = k_1 v + k_2 v^{1/2} \tag{6}$$

Where *i(V)* is the current at a fixed potential. The constants k_1 & k_2 are given by the slope and intercept of a linear regression plot between current and $v^{1/2}$, respectively. CV curves at 40 mV s^{-1} were further analysed to study the reaction kinetic mechanism of the prepared samples as shown in Figure 5.8. We can see from the Figure 5.8 (a, b, c) that diffusive contribution is dominant for the basic electrolyte (i.e., 1M KOH). It can be attributed to faradic reactions that occur during charging/discharging. Oxidation and reduction peaks can be seen in the region of 0.2-0.3 V resulting from the oxidation/reduction of metallic cobalt in the electrode material [24]. In neutral electrolyte (1 M Na_2SO_4), diffusive behaviour is dominant for TZ-700, but capacitive behaviour is dominant for TZ-800 and TZ-900. It is attributed to smaller surface area of TZ-800 and TZ-900 resulting in lesser diffusion of solvated ions while TZ-700 has higher surface area. Due to very small ionic radius of H^+ ions in the acidic solution, formation of electric double layer is easier and results in faster reaction kinetics [25, 26]. In H_2SO_4, capacitive behaviour is prominent in TZ-900 (92% as mentioned in Table 4) with fast EDLC layer formation by solvated H^+ and SO_4^{-2} ions resulting in highest specific capacitance.

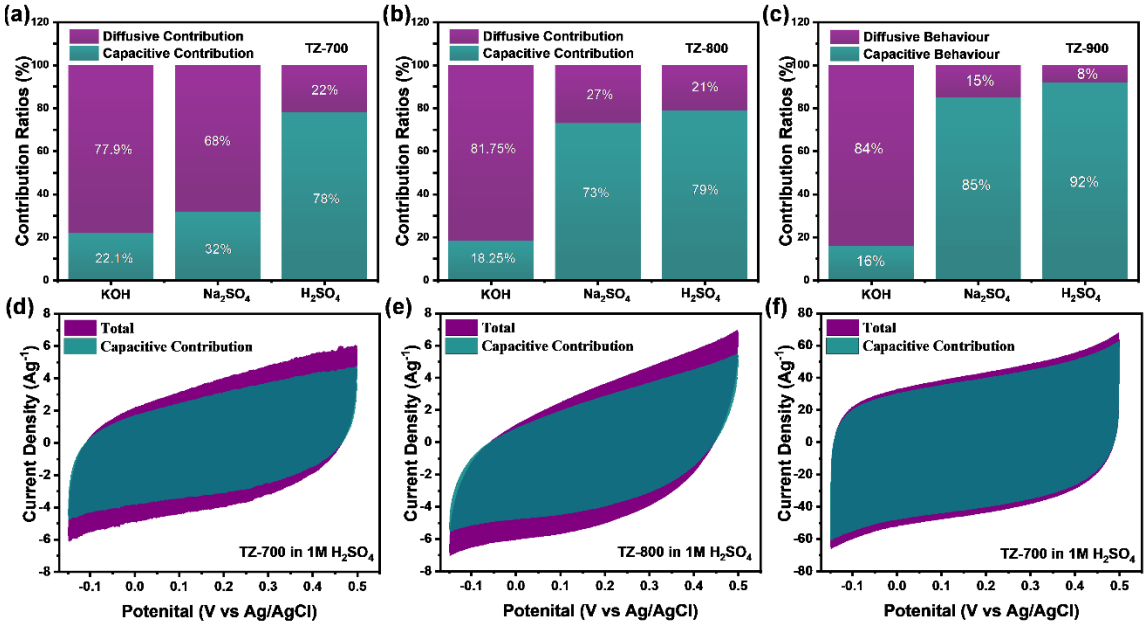

Figure 5-7. Comparison of total current vs capacitive current at 40 mV s^{-1} for (a) TZ-700 (b) TZ-800 and (c) TZ-900. (d-f) Capacitive current contribution for TZ-700, TZ-800, and TZ-900 in 1M H_2SO_4

5.2.4 Cyclic Stability

Cyclic Stability of the best performing electrode i.e., TZ-900 was tested in 1M H_2SO_4 for 10,000 cycles. It has shown an 84% specific capacitance retention at 10 A g^{-1}. Fig 5.10 (d) shows the percentage retention with first cycle and 10,000th cycle. It has been reported that materials with EDLC behaviour tend to have a higher cyclic stability as compared to materials showing faradic reactions [27, 28]. Titania in the prepared sample behaves like EDLC, therefore a high specific capacitance retention at high current density is observed.

5.2.5 Electrochemical Impedance Spectroscopy

EIS was carried out to investigate further the charge transfer kinetics and impedance mechanism of prepared electrodes. The Nyquist plot is given in figure 5.10 (a, b, c) and consists of 3 components. At high frequency, the point arises where the plot intercepts on x-axis, it is ohmic or solution resistance (R_s). The semicircle component present at high-medium frequency is contribution of charge transfer resistance (R_{ct}) and solution resistance (R_s). The linear fitted line at the end is called the Warburg resistance (R_w). The equivalent circuit is shown in the inset of Figure 5.10 (a, b, and c). R_s values in the basic electrolyte are 13.67 Ω, 13.5 Ω and 11.24 Ω which is lowest for the sample TZ-900 as

shown in the inset of Fig 5.10 (a). R_s values in the acidic electrolyte are 6.03 Ω, 5.98 Ω &5.7844 Ω which again is lowest for the sample TZ-900 as shown in the inset of Fig 5.10 (b). R_s values in the neutral electrolyte are 18.24 Ω, 18.14 Ω and 18.11 Ω which as well is lowest for TZ-900 as shown.

Sample	**Electrolyte**	**Rs**	**Rct**
TZ-700	1M KOH	13.67	31.69
TZ-800	1M KOH	13.5	28.12
TZ-900	1M KOH	11.24	19.38
TZ-700	1M H_2SO_4	6.03	25.67
TZ-800	1M H_2SO_4	5.98	9.346
TZ-900	1M H_2SO_4	5.7844	8.551
TZ-700	1M Na_2SO_4	18.24	47.19
TZ-800	1M Na_2SO_4	18.14	27.72
TZ-900	1M Na_2SO_4	18.11	13.1

The smaller solution resistance value is the reason behind higher electrochemical activity in acidic medium. R_{ct} values from the equivalent circuit are 31.69 Ω, 28.12 Ω and 19.38 Ω for TZ-700, TZ-800, and TZ-900 in 1M KOH. R_{ct} values estimated from the equivalent circuit are 25.67 Ω, 9.346 Ω and 8.551 Ω for TZ-700, TZ-800, and TZ-900 in 1M H_2SO_4. R_{ct} values estimated from the equivalent circuit are 47.19 Ω, 27.72 Ω and 13.1 Ω for TZ-700, TZ-800, and TZ-900 in 1M Na_2SO_4. These results show that overall charge transfer resistance is smallest for the acidic electrolyte. Moreover, in acidic electrolyte, TZ-900 electrode has the lowest R_{ct} .The TZ-900 electrode has the smallest R_{ct} value due to the small semi-circle diameter than other electrodes in the high frequency region of Nyquist plot shown in inset of Figure 5.10 (b). In the acidic medium, R_{ct} is lowest for TZ-900 resulting in quick formation of electric double layer by accumulation of opposite charges on electrode surface. It contributes towards the higher specific capacitance of TZ-900.

Table 5. 3 Rs and Rct values as calculated from Randell's circuit

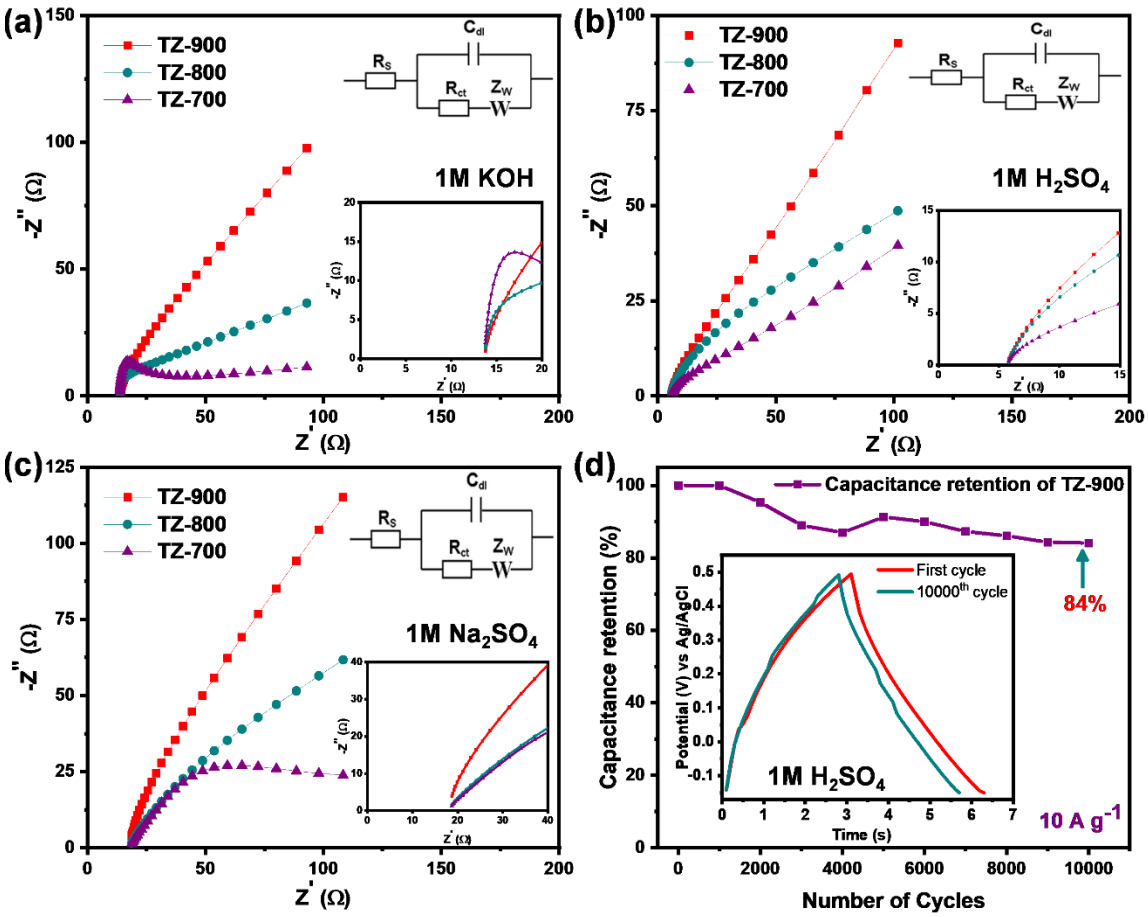

Figure 5-8. (a) Nyquist plots of TZ-700, TZ-800, and TZ-900 in (a) 1M KOH (b)1M H_2SO_4 and (c) 1M Na_2SO_4.

Table 5-4. Comparison of similar electrodes specific capacitance from literature

Electrode Material	**Specific Capacitance (F g^{-1})**	**Current Density (A g^{-1})/ Scan Rate (mV s^{-1})**	**Electrolyte**	**Ref.**
rGO-TiO_2-MoO_3	472	1 A g^{-1}	2 M Na_2SO_4	[29]
Co_3O_4@C	251	1 A g^{-1}	1 M KOH	[31]

$AC/TiO_2/Co_3O_4$	946	5 mV s^{-1}	6 M KOH	[32]
$N–Ti_3C_2T_x/C/CuS$	1205	1 A g^{-1}	1 M KOH	[33]
$N\text{-graphene}/Co_3O_4$	90	20 mV s^{-1}	3 M KOH	[34]
TZ-900	1617	0.5 A g^{-1}	1 M H_2SO_4	This work

Summary

All the results obtained during the research are discussed in this chapter. Characterization results of TGA, XRD, SEM, EDS, TEM, XPS, CV, GCD and EIS are supported with facts from previous studies and justified to understand the morphology, structure, composition, thermal stability, functional groups, and porosity of the synthesized materials. Electrochemical results of the synthesized electrodes are discussed at the end. All the results are presented after comparison with the literature and are supported in the light of properties from characterization techniques.

List of references

[1] Yu, Y., et al., *Ti3+-self-doped TiO2 with multiple crystal-phases anchored on acid-pickled ZIF-67-derived Co3O4@ N-doped graphitized-carbon as a durable catalyst for oxygen reduction in alkaline and acid media.* Chemical Engineering Journal, 2021. **403**: p. 126441.

[2] Sun, X., et al., *Decorating MOF-derived nanoporous Co/C in chain-like polypyrrole (PPy) aerogel: a lightweight material with excellent electromagnetic absorption.* Materials, 2018. **11**(5): p. 781.

[3] Guo, Y., et al., *Effect of various carbonization temperatures on ZIF-67 derived nanoporous carbons.* Bulletin of the Chemical Society of Japan, 2017. **90**(8): p. 939-942.

[4] Li, D.-P., et al., *Development of a hollow carbon sphere absorber displaying the multiple-reflection effect to attenuate electromagnetic waves.* RSC advances, 2017. **7**(60): p. 37983-37989.

[5] Yang, J., et al., *Improving oxygen reduction reaction of microbial fuel cell by titanium dioxide attaching to dual metal organic frameworks as cathode.* Bioresource Technology, 2022. **349**: p. 126851.

[6] Wang, L., et al., *Co3O4 hollow nanospheres/carbon-assembled mesoporous polyhedron with internal bubbles encapsulating TiO2 nanosphere for high-performance lithium ion batteries.* Nanotechnology, 2019. **30**(35): p. 355401.

[7] Abbas, M., et al., *Fabrication of cobalt doped titania for enhanced oxygen evolution reaction.* Molecular Catalysis, 2020. **488**: p. 110894.

[8] Li, L., et al., *Recent discovery of a multifunctional metallo-organic precursor for fabricating Co 3 O 4/N-doped porous carbon by one-step in situ pyrolysis as an anode material for Li-ion batteries.* Journal of Materials Science, 2021. **56**: p. 1590-1599.

[9] Davoodi, M., et al., *Cobalt metal–organic framework-based ZIF-67 for the trace determination of herbicide molinate by ion mobility spectrometry: investigation of different morphologies.* RSC advances, 2021. **11**(5): p. 2643-2655.

[10] Bo, S., et al., *Interior engineering of seaweed-derived N-doped versatile carbonaceous beads with Co x O y for universal organic pollutant degradation.* RSC advances, 2019. **9**(9): p. 5009-5024.

[11] Boppella, R., et al., *Composite hollow nanostructures composed of carbon-coated Ti 3+ self-doped TiO 2-reduced graphene oxide as an efficient electrocatalyst for oxygen reduction.* Journal of Materials Chemistry A, 2017. **5**(15): p. 7072-7080.

[12] Ghoshal, S., et al., *ZIF 67 based highly active electrocatalysts as oxygen electrodes in water electrolyzer.* ACS Applied Energy Materials, 2019. **2**(8): p. 5568-5576.

[13] Zhong, G., D. Liu, and J. Zhang, *The application of ZIF-67 and its derivatives: adsorption, separation, electrochemistry and catalysts.* Journal of Materials Chemistry A, 2018. **6**(5): p. 1887-1899.

[14] Panchariya, D.K., et al., *Core–shell zeolitic imidazolate frameworks for enhanced hydrogen storage.* ACS omega, 2018. **3**(1): p. 167-175.

[15] Raza, M.A., et al., *CoS2/MnS2 co-doped ZIF-derived nitrogen doped high surface area carbon-based electrode for high-performance supercapacitors.* Electrochimica Acta, 2022. **407**: p. 139914.

[16] Chen, X., et al., *ZIF-67-derived Mn doped Co9S8 supported on N-Enriched porous carbon polyhedron as an efficient electrocatalyst for oxygen evolution reaction.* International Journal of Hydrogen Energy, 2021. **46**(78): p. 38724-38732.

[17] Frackowiak, E., F.J.P.W.-V.V.G. Béguin, and Co, *Supercapacitors: Materials, Systems and Applications.* 2013.

[18] Zheng, S., et al., *Transition-metal (Fe, Co, Ni) based metal-organic frameworks for electrochemical energy storage.* 2017. **7**(18): p. 1602733.

[19] Zheng, S., H. Xue, and H. Pang, *Supercapacitors based on metal coordination materials.* Coordination Chemistry Reviews, 2018. **373**: p. 2-21.

[20] Suwandi, D.A., et al. *Effect of Aqueous Electrolyte to the Supercapacitor Electrode Performance Made from Sugar Palm Fronds Waste*. in *Journal of Physics: Conference Series*. 2021. IOP Publishing.

[21] Zhang, L., et al., *A review of redox electrolytes for supercapacitors.* Frontiers in Chemistry, 2020. **8**: p. 413.

[22] Ramachandran, R. and F. Wang, *Electrochemical capacitor performance: Influence of aqueous electrolytes.* Supercapacitors-Theor Pract Solut InTech, 2018: p. 51-68.

[23] Ramadoss, A. and S.J. Kim, *Improved activity of a graphene–TiO2 hybrid electrode in an electrochemical supercapacitor.* Carbon, 2013. **63**: p. 434-445.

[24] Iqbal, M.Z., et al., *Capacitive and diffusive contribution in strontium phosphide-polyaniline based supercapattery.* Journal of Energy Storage, 2020. **29**: p. 101324.

[25] Bao, W., et al., *Fabrication and electrical double-layer capacitance performance of interconnected and independent titania nanotube array.* Materials Research Innovations, 2021. **25**(1): p. 8-15.

[26] Pholauyphon, W., et al., *High-performance supercapacitors using carbon dots/titanium dioxide composite electrodes and carbon dot-added sulfuric acid electrolyte.* Journal of Electroanalytical Chemistry, 2022. **910**: p. 116177.

[27] Thulasi, K.M., et al., *Supercapacitor electrodes based on modified titania nanotube arrays on flexible substrates.* International Journal of Materials Research, 2021. **112**(12): p. 937-944.

[28] Wu, Q., et al., *Cyclic stability of supercapacitors: materials, energy storage mechanism, test methods, and device.* Journal of Materials Chemistry A, 2021. **9**(43): p. 24094-24147.

[29] Britto, S., et al., *Preparation and electrochemical validation of rGO-TiO2-MoO3 ternary nanocomposite for efficient supercapacitor electrode.* Diamond and Related Materials, 2022. **122**: p. 108798.

[30] Kolathodi, M.S. and T.S. Natarajan, *Development of high-performance flexible solid state supercapacitor based on activated carbon and electrospun TiO2 nanofibers.* Scripta Materialia, 2015. **101**: p. 84-86.

[31] Gong, H., et al., *In Situ Construction of ZIF-67-Derived Hybrid Tricobalt Tetraoxide@ Carbon for Supercapacitor.* Nanomaterials, 2022. **12**(9): p. 1571.

[32] Sireng, K., *Fish bladder-based activated porous carbon/co3o4/tio2 composite electrodes for supercapacitors*. 2020, NM-AIST.

[33] Deng, Y., et al., *A novel electrode hybrid of N–Ti3C2Tx/C/CuS fabricated using ZIF-67 as an intermediate derivation for superhigh electrochemical properties of*

supercapacitors. Journal of Materials Research and Technology, 2022. **19**: p. 3507-3520.

[34] Chen, T.-Y., et al., *Novel direct growth of ZIF-67 derived Co3O4 and N-doped carbon composites on carbon cloth as supercapacitor electrodes.* Journal of Colloid and Interface Science, 2022. **608**: p. 493-503.

Chapter 6: Conclusions and Recommendations

6.1 Conclusions

The quaternary porous composite derived from ZIF-67 structure is successfully synthesized with globular-like morphology using a simple co-precipitation method in conjunction with solvothermal addition of titania. TiO_2 in ZIF-67 porous structure has significantly improved the reaction kinetics and stability of electrochemical activity along with retention of porous carbon structure. XRD, XPS, and HRTEM are collectively used to find the phases and planes in the samples TZ-700 to TZ-900. A closely packed configuration of a-TiO_2, metallic cobalt and cobalt oxide planes is observed through HRTEM. The electrochemical profile is evaluated in three electrode assembly through CV, GCD and EIS measurements. Electrochemical performance of this quaternary composite depends electrolyte composition. Acidic, basic and neutral aqueous electrolytes are studied in this work which reveals the higher current response in the acidic electrolyte. It is due to smaller solvated ion radius of H^+ ion in H_2SO_4 resulting in capacitive behaviour domination and quick formation of EDLC. An EDLC supercapacitor with a specific capacitance of 1617 F g^{-1} in H_2SO_4 is obtained in three-electrode configuration using TZ-900 electrode material with up to 84% stability after 10,000 cycles at 10 A g^{-1}. This increased capacitance is attributed to the synergistic coordination between Co^0, Co^{+3}, and Ti^{+4}. Moreover, H^+ in acidic electrolyte facilitates the formation of EDLC layer resulting in faster kinetics and greater capacitive contribution. Furthermore, the incorporation of titania rods, spheres, or fibers into the hexagonal structure of ZIF-67 is suggested to improve the electrochemical performance along with fabrication of two-electrode supercapacitor device.

6.2 Recommendations

The electrochemical performance and efficiency of supercapacitors for energy storage applications can be increased by exploring new combinations of materials to be employed as electrodes, in addition to the informed selection of electrolytes. The following recommendations are presented to address the shortcomings in the research regarding the electrode materials for supercapacitors:

- Focus of the future research should be towards the various transition metals and their sulfides in addition to the metal oxides to be used as efficient electrode materials for supercapacitors.
- Graphene based materials and composites should be explored to enhance the stretch, flexibility and electrochemical performance of the supercapacitors.
- In contrast to Li-ion batteries, supercapacitors lack the required energy density. Therefore, research is required in the direction of hybrid batteries or hybrid capacitors, i.e., combination of Li-ion and supercapacitor assemblies, to ensure maximum power density and energy density simultaneously.
- MOFs provide the basic framework for such applications, as they demonstrate large surface areas as compared to other compounds and composites. Research should be done to explore the various existing MOFs compounds and their derivatives.

Appendix 1- Publications

Abstract

A quaternary composite has been synthesized from metal-organic frameworks (MOFs), one of the widely used precursors for the development of electrode material for supercapacitors. ZIF-67 template has been synthesized using a typical co-precipitation method followed by addition of titania in a solvothermal reactor. Three quaternary composites derived from ZIF-67 pyrolyzed at 700 ℃, 800 ℃ and 900 ℃ are synthesized using simple co-precipitation method followed by solvothermal reaction. The morphological analysis revealed a nearly globular morphology for composite prepared at temperature 900 ℃ (TZ-900). An increased degree of graphitization for carbon in the sample pyrolyzed at high temperature as confirmed using Raman spectroscopy can be attributed to better electrochemical performance. Three aqueous electrolytic media are used to study the electrochemical behavior of prepared samples comprising 1M KOH, 1M H_2SO_4, and 1M Na_2SO_4. The prepared electrodes, TZ-700, TZ-800, and TZ-900 exhibited a specific capacitance of 303, 615, and 1617 F g^{-1} in the acidic media at 0.5 A g^{-1}. Cyclic stability run for 10,000 cycles with TZ-900 electrode showed a specific capacitance retention of 84% at a current density of 10 A g^{-1}. X-ray photoelectron spectroscopy & transmission electron microscopy further helped to examine the synergistic effect of metallic cobalt, Co (II), Co (III) and titanium ions in the nano-graphitic carbon matrix.

Journal name: Electrochimica Acta

Status: Under Review